nature biotechnology

ARTICLES

https://doi.org/10.1038/s41587-020-00781-8

Targeting herpes simplex virus with CRISPR–Cas9 cures herpetic stromal keratitis in mice

Di Yin[1,6], Sikai Ling[1,6], Dawei Wang[2,6], Yao Dai[1], Hao Jiang[3,4], Xujiao Zhou[3], Soren R. Paludan[5], Jiaxu Hong[3,4] ✉ and Yujia Cai[1] ✉

Herpes simplex virus type 1 (HSV-1) is a leading cause of infectious blindness. Current treatments for HSV-1 do not eliminate the virus from the site of infection or latent reservoirs in the trigeminal ganglia. Here, we target HSV-1 genomes directly using mRNA-carrying lentiviral particles that simultaneously deliver SpCas9 mRNA and viral-gene-targeting guide RNAs (designated HSV-1-erasing lentiviral particles, termed HELP). We show that HELP efficiently blocks HSV-1 replication and the occurrence of herpetic stromal keratitis (HSK) in three different infection models. HELP was capable of eliminating the viral reservoir via retrograde transport from corneas to trigeminal ganglia. Additionally, HELP inhibited viral replication in human-derived corneas without causing off-target effects, as determined by whole-genome sequencing. These results support the potential clinical utility of HELP for treating refractory HSK.

HSV-1 is among the most common human viruses, with 50–80% of the world population being seropositive[1]. It belongs to the alpha subfamily of herpesviruses, which are enveloped viruses carrying double-stranded DNA and are capable of establishing latent infections in sensory neurons[2]. HSV-1 infection can cause a wide variety of diseases, including herpes simplex encephalitis, which has a high mortality rate if untreated[3]. HSV-1 infection in the cornea can cause HSK, which is the leading factor for infectious blindness[4]. After primary infection and productive replication in corneal epithelium, HSV-1 is transported through ophthalmic nerves in a retrograde direction to the trigeminal ganglia (TG), where the virus establishes a latent reservoir that persists throughout an individual's lifetime[5]. Under certain conditions, including immunosuppression, the latent viruses in the TG can be reactivated, leading to recurrence and aggravation of disease. Typical blinding HSK develops subsequently to infection in the eye, at which point virus can often not be detected[6]. Most of the tissue damage occurring in human corneas during HSK is immune mediated rather than a direct viral cytopathic effect[7]. Globally, it is estimated that 1.5 million episodes of ocular HSV occur each year and 40,000 people develop visual disability[4].

Despite the high prevalence, there is no vaccine currently available for HSV infection[8,9]. The first-line treatment option for HSV-1 infection is acyclovir (ACV). This compound was developed nearly half a century ago and analogs have subsequently been made, all targeting the viral DNA polymerase. In specific patient groups, including immunocompromised individuals and individuals receiving chronic antiviral prophylaxis, drug resistance occurs frequently[10–12]. Alternative strategies, including small molecules that inhibit the viral helicase–primase complex, antibodies and peptides, are still under development[13–15]. Recently, Jaishankar et al. reported that BX795, a commonly used inhibitor of TANK-binding kinase 1, blocks HSV-1 infection in vivo by targeting Akt phosphorylation in infected cells[16]. However, none of these strategies can remove the existing virus and modulate its reservoir in the TG, and they are therefore incapable of preventing recurrence.

CRISPR targets genomes directly and has been very successful in treating genetic diseases in preclinical studies[17–22]. About 2 years ago, the US Food and Drug Administration approved CRISPR for phase I/II trials to treat β-thalassemia, sickle cell disease and Leber congenital amaurosis type 10 (ClinicalTials.gov: NCT04208529, NCT03745287 and NCT03872479). Its therapeutic potential on infectious diseases is promising. Dash et al. demonstrated viral clearance in latent infectious reservoirs in human immunodeficiency virus type 1 (HIV-1)-infected humanized mice by combining antiviral prodrugs and CRISPR[23]. However, to the best of our knowledge, no investigational new drug application has been registered for infectious diseases. This reflects the challenge of delivering CRISPR to infection sites and especially to viral reservoirs[24]. One study delivered an HSV-1-targeting endonuclease using adeno-associated virus (AAV) in a mouse model of latent HSV infection; however, this study revealed neither a detectable loss of viral genome nor therapeutic efficacy[25]. Recently, the same group showed detectable elimination of latent genomes and therapeutic efficacy by using an improved AAV vector and two meganucleases targeting the HSV genome[26]. So far, the anti-HSV activity of CRISPR has only been characterized in vitro, and no studies have shown the therapeutic efficacy of CRISPR against HSK in vivo[27,28].

In this study, we developed HELP and showed its therapeutic efficacy in three different HSK models and in human-derived corneas. Furthermore, we found that HELP was capable of modulating the HSV-1 reservoir in the TG. Corneas maintained a healthy status after intracorneal injection of HELP, as shown by a variety of clinically relevant assays. Cas9 expression from HELP only lasted for 3 d in vivo, and no off-target effects were detected in the coding regions of the mouse and human genomes. Taken together, our study supports the clinical translation of HELP for treating

[1]Key Laboratory of Systems Biomedicine (Ministry of Education), Shanghai Center for Systems Biomedicine, Shanghai Jiao Tong University, Shanghai, China. [2]National Research Center for Translational Medicine, Ruijin Hospital Affiliated to Shanghai Jiao Tong University School of Medicine, Shanghai, China. [3]Department of Ophthalmology and Vision Science, Shanghai Eye, Ear, Nose and Throat Hospital, Fudan University, Shanghai, China. [4]Department of Ophthalmology, The Affiliated Hospital of Guizhou Medical University, Guiyang, China. [5]Department of Biomedicine, Aarhus University, Aarhus, Denmark. [6]These authors contributed equally: Di Yin, Sikai Ling, Dawei Wang. ✉e-mail: jiaxu_hong@163.com; yujia.cai@sjtu.edu.cn

refractory HSK, which has been resistant to conventional drugs and corneal transplantation.

Results

HELP blocks HSV-1 replication in vitro. In this study, we designed a guide RNA (gRNA) expression cassette simultaneously targeting two essential genes of HSV-1, *UL8* and *UL29* (refs. [29,30]), and co-packaged it with SpCas9 mRNA in an mRNA-carrying lentiviral particle (mLP) via the specific binding of pac site-containing SpCas9 mRNA to bacteriophage-derived MS2 coat protein located at the N terminus of lentiviral Gag and GagPol polyproteins (Fig. 1a–c). The MS2 coat protein specifically recognizes and interacts with the pac site-containing SpCas9 mRNA and co-packages it into the lentiviral particle during viral assembly. The gRNA expression cassette is reverse transcribed and maintained as circular episomal DNA, corresponding to an integration-defective lentiviral vector (Fig. 1b). As the *UL8* gRNA is cloned into the ΔU3 region of the long terminal repeat (LTR), it is copied from the 3′ LTR to the 5′ LTR during reverse transcription (Fig. 1b). We produced HELP by cotransfection of six plasmids into 293T cells and harvested the particles by ultracentrifugation (Fig. 1c). As controls, we also produced mLPs with a single-gRNA expression cassette, for *UL8*, *UL29* or a scrambled sequence (non-targeting gRNA). To verify whether HELP was indeed capable of inhibiting HSV-1, 293T cells were transduced with HELP for 24 h and infected with HSV-1 (HSV-1–GFP). The supernatants were harvested 1 d and 2 d after HSV-1 infection and subjected to a virus yield assay. We found inhibitory effects for all viral gene-targeting mLPs, with the *UL8*/*UL29* co-targeting HELP being the most efficient (Fig. 1d and Supplementary Fig. 1). The average copy number of Cas9 mRNA in HELP was 3.5 (Supplementary Fig. 2). Additionally, we conducted a dose–response experiment for HELP, which showed an increasing level of virus inhibition that reached saturation at 400 ng of p24 (Fig. 1e). We therefore chose HELP in all the subsequent experiments.

HSV-1 infection is sensitive to type I interferons (IFNs) induced by pathogen-associated molecular patterns, even in the absence of gene editing (Supplementary Fig. 3; ref. [31]). To exclude a necessity for type I IFNs here, we evaluated the antiviral activity of HELP in both wild-type and interferon alpha and beta receptor subunit 2 (*IFNAR2*)-knockout HaCaT cells. We found that HELP, but not the scrambled control, significantly inhibited HSV-1 replication in both cell lines (Fig. 1f,g). Furthermore, we analyzed the *UL8* and *UL29* loci and found that, on average, the indel frequency was about 40% for *UL8* while only 7% for *UL29* (Fig. 1h). The indel rate in *UL29* was relatively low. As ICP8 (encoded by *UL29*) plays multifunctional roles in the viral life cycle, including in viral DNA synthesis, we reasoned that mutations in *UL29* make the virus unable to replicate and tend to be underestimated[30]. Indeed, when using plasmids containing *UL8* and *UL29* sequences as the targets, we obtained even higher indel rates with *UL29* gRNA than with *UL8* gRNA (Fig. 1i). Notably, the antiviral activity of HELP is underestimated using PCR-based indel analysis, as not all the cleavage outcomes, for example, unrepaired double-strand breaks or large deletions, can be amplified (Supplementary Fig. 4). Also, we found that HELP did not provoke innate immune sensing, in contrast to HSV-1 strains, which were all sensed by THP-1-derived macrophages at a multiplicity of infection (MOI) of 1 and induced a moderate but significant IFN response (Supplementary Fig. 5). Together, these data suggest that HELP inhibits HSV-1 through DNA disruption but not through a type I IFN-dependent innate immune response.

The corneal stroma is highly linked to keratitis recurrence[32]. The stroma is rich with nerve trunks that originate from the TG where HSV-1 maintains latency[33]. Therefore, we explored whether HELP was functional in primary corneal stromal cells from mice. Primary stromal cells were transduced with non-GFP HELP for 24 h and then infected with HSV-1–GFP. We found that HELP potently suppressed GFP expression as well as viral replication using both low and high MOIs at either 24 h or 48 h after infection, while the scrambled control did not show any protective effects (Fig. 1j–m).

HELP blocks HSV-1 infection of corneas and neurons in the prevention model. Persisting nuclease expression may bring additional risks. From a safety perspective, transient nuclease exposure is desired for CRISPR therapeutics. However, it is unclear whether transient Cas9 expression can control HSK, as HSV-1 propagates quickly (about 18 h for the lytic replication cycle). It is difficult for the CRISPR machinery to remove every HSV-1 genome. On the other hand, HSV-1 encounters harsh antiviral responses in vivo. Here, we hypothesize that reducing the viral load to a certain level is sufficient to control the virus in vivo. To verify this, we performed dose–response experiments of HSV-1 infection on scarified corneas of mice. Indeed, only when the HSV-1 load was over 2×10^4 plaque-forming units (p.f.u.) did the decreased viability, weight loss and symptoms of keratitis develop (Supplementary Fig. 6).

We then set out to investigate the potential of HELP as a new HSK therapeutic in vivo. To identify the kinetics of HSV-1 infection in our HSK model, we visualized HSV-1 using confocal imaging and found that the virus progressively disseminated from the superficial side to the deeper side of corneal stroma during the time course from 12 h to 8 d post-infection (d.p.i.; Supplementary Fig. 7). The experimental setup is illustrated in Fig. 2a. HELP was administrated by intrastromal injection to corneas 1 d before infection with HSV-1 strain 17syn+ (Supplementary Fig. 8). We first performed deep sequencing to determine the on-target activity of HELP on the HSV-1 genome and the off-target effects on the mouse genome. The indels induced by HELP occurred at rates of approximately 7% for the *UL8* locus and 5% for the *UL29* locus, while no off-target sites were found for either gRNA (Fig. 2b,c). Notably, Cas9 expression only lasted for 3 d both in vitro and in vivo, which might minimize the off-target activity of HELP (Supplementary Fig. 9). Next, we performed confocal imaging to assess HSV-1 replication and HELP distribution in the corneas of mice, which were indicated by the viral capsid protein VP5 and GFP, respectively. We found that HSV-1 was actively replicating in the corneal stroma in mock- and scrambled control-treated mice, while it was barely detectable after HELP treatment (Fig. 2d). Accordingly, HELP were evenly distributed in all corneal structures from the epithelium and stroma to the endothelium (Fig. 2d). To assess whether HELP treatment blocks the transmission of HSV-1 from corneal epithelium to the peripheral and central nervous system, eye, TG and brain samples from all infected mice were collected and examined for HSV-1 genome copy number and infectious virus. In all samples, the viral load was significantly reduced after HELP treatment (Fig. 2e–j). Additionally, we performed confocal imaging of the whole brain and TG. In agreement with the quantitative PCR (qPCR) and p.f.u. analyses, we found that HELP diminished HSV-1 viral load to an almost undetectable level in both the brain and TG (Fig. 2k,l). Tissue distribution is an important safety index for in vivo gene therapy. Therefore, we evaluated the dissemination of HELP in the whole body, finding that HELP were highly restricted to the eyes and did not localize to other organs, including reproductive organs (Supplementary Fig. 10). Interestingly, although they were injected in the corneas, we also detected HELP in the TG, supporting the concept of retrograde delivery of CRISPR machinery from neuronal termini in the corneas to the neuronal cell body in the TG (Supplementary Fig. 10). This finding was further supported by detection of HELP in the TG by confocal imaging (Fig. 2m).

HELP suppresses HSV-1-associated disease pathologies in the prevention model. To determine disease development and therapeutic efficacy, we monitored the clinical signs of acute ocular herpes infection and scored them in a blinded fashion (Fig. 3a).

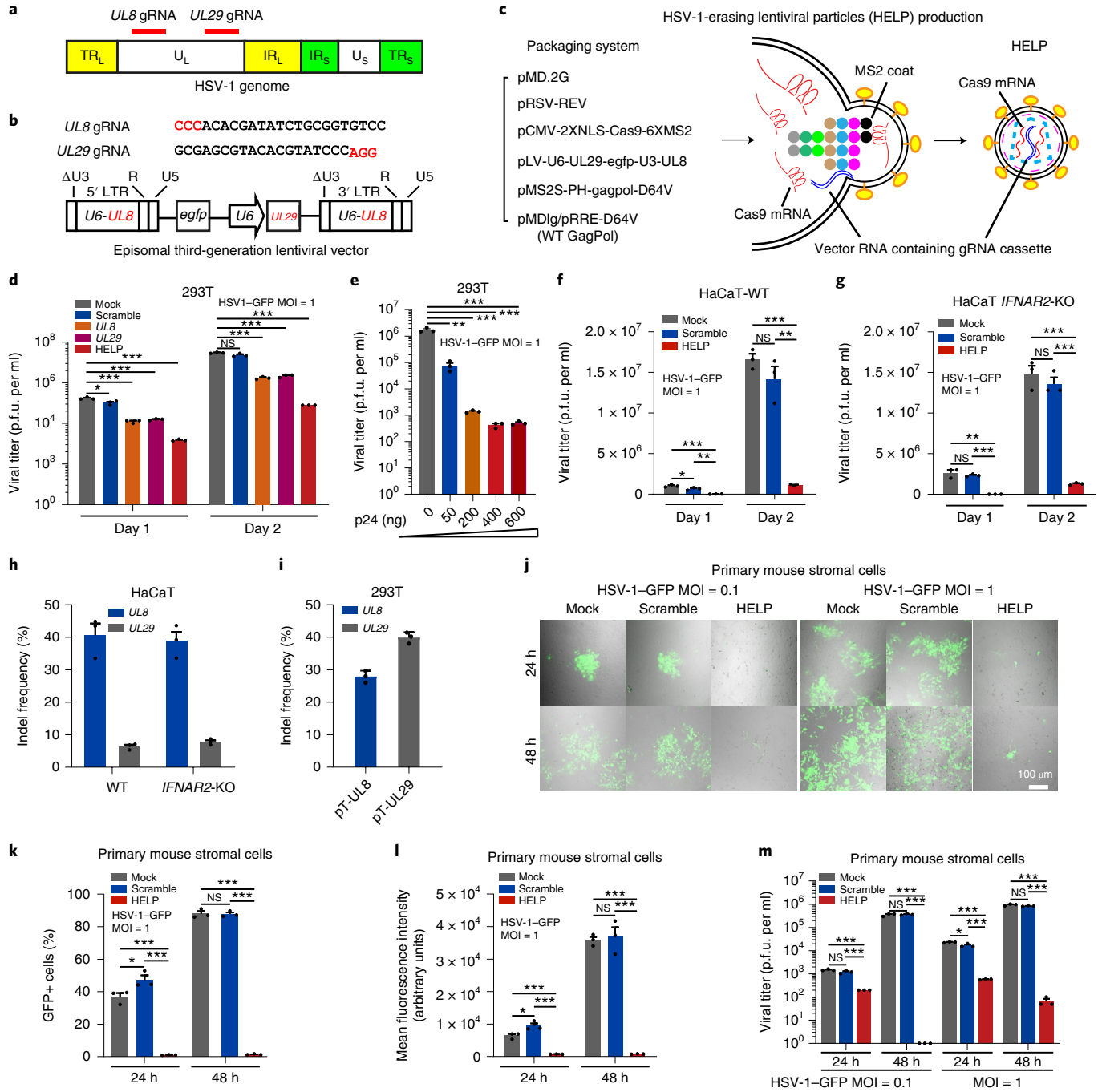

Fig. 1 | HELP blocks HSV-1 replication in vitro. a, Schematic representation of the HSV-1 genome and gRNA loci. TR_L, terminal repeat long; IR_L, internal repeat long; U_L, unique long; IR_S, internal repeat short; TR_S, terminal repeat short; U_S, unique short. **b**, The gRNA sequences and expression cassettes for HELP. **c**, Schematic illustration of HELP production. Colored dots represent the main components of lentiviral Gag and GagPol polyproteins. Gag is composed of matrix (MA), capsid (CA) and nucleocapsid (NC), whereas Pol consists of protease (PR), reverse transcriptase (RT) and integrase (IN). **d**–**g**, The antiviral activity of HELP in different cell lines. In **d**, mock versus scramble, *UL8*, *UL29* and HELP, $P = 0.0220$, 0.0003, 0.0003 and 0.0002, respectively, on day 1; $P < 0.0001$ on day 2. In **e**, mock versus 50 ng p24, $P = 0.0011$; $P = 0.0009$ for all other comparisons. In **f**, HELP versus mock and scramble, $P = 0.0003$ and 0.0019, respectively, on day 1; $P < 0.0001$ and $P = 0.0011$, respectively, on day 2. Mock versus scramble, $P = 0.0420$ on day 1. In **g**, HELP versus mock and scramble, $P = 0.0013$ and $P < 0.0001$, respectively, on day 1; $P = 0.0002$ and 0.0001, respectively, on day 2. **h**, TIDE analysis of indels in the HSV-1 genome. Viral DNA was from day 2 samples in **f** and **g**. **i**, TIDE analysis of indels in plasmids containing *UL8* and *UL29* target sequence, respectively. **j**–**m**, Antiviral activity in primary mouse corneal stromal cells as measured by confocal microscopy (**j**), flow cytometry (**k**,**l**) and p.f.u. analysis (**m**). In **k**, mock versus HELP, $P = 0.0001$ at 24 h; $P < 0.0001$ for all other comparisons. In **l**, $^*P = 0.0380$, $^{***}P = 0.0005$, $^{***}P = 0.0004$, $^{***}P < 0.0001$ and $^{***}P = 0.0003$, left to right. In **m**, $^{***}P < 0.0001$, $^{***}P = 0.0010$, $^{***}P = 0.0002$, $^{***}P < 0.0001$, $^*P = 0.0236$, $^{***}P < 0.0001$, $^{***}P = 0.0006$, $^{***}P < 0.0001$ and $^{***}P < 0.0001$, left to right. In **j**, images are representative of three independent biological replicates in one experiment. The gating strategy is provided in Supplementary Fig. 20. Data and error bars represent mean ± s.e.m. from three biologically independent replicates. Unpaired two-tailed Student's *t* tests. NS, not significant; WT, wild type; KO, knockout.

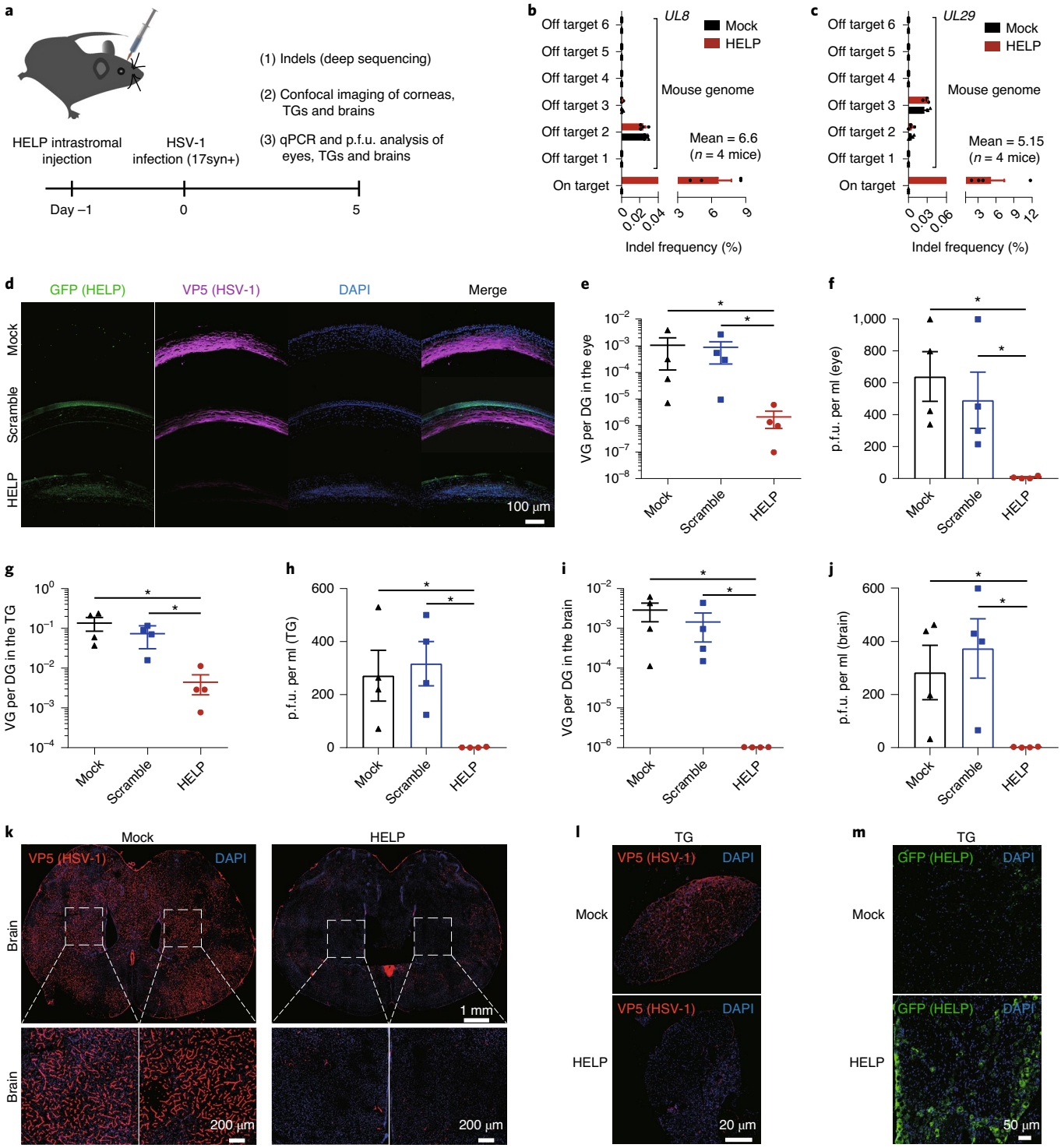

Fig. 2 | HELP blocks HSV-1 infection of corneas and neurons in a prevention model. a, Flowchart for evaluating the antiviral effects of HELP in vivo. p24 HELP (100 ng), scrambled control mLP or 2 μl PBS (mock) was injected into the corneas of mice by intrastromal injection. After 24 h, the mice were infected with HSV-1 17syn+ (2×10^6 p.f.u. per eye). **b**, Deep sequencing analysis of on-target effects in HSV-1 and off-target effects in the mouse genome for *UL8* gRNA; $n=4$ mice. **c**, Deep-sequencing analysis of on-target effects in HSV-1 and off-target effects in the mouse genome for *UL29* gRNA; $n=4$ mice. **d**, Confocal imaging of HSV-1 and HELP in corneas. Mouse corneal sections were incubated with both anti-GFP (HELP) and anti-HSV-1 (VP5) antibodies. **e**, qPCR analysis of HSV-1 dissemination in the eye. **f**, p.f.u. analysis of HSV-1 dissemination in the eye. **g**, qPCR analysis of HSV-1 dissemination in the TG. **h**, P.f.u. analysis of HSV-1 dissemination in the TG. **i**, qPCR analysis of HSV-1 dissemination in the brain. **j**, P.f.u. analysis of HSV-1 dissemination in the brain. In **e**–**j**, the abundance of HSV-1 is shown as the number of viral genomes (VG) per diploid genome (DG); $n=4$ mice; $^*P=0.0286$. **k**,**l**, Confocal analysis of HSV-1 in the whole brain (**k**) and TG (**l**). **m**, Confocal analysis of HELP in the TG after intracorneal injection. Data and error bars represent mean ± s.e.m.; unpaired two-tailed Mann–Whitney tests. The experiments were repeated twice with similar results.

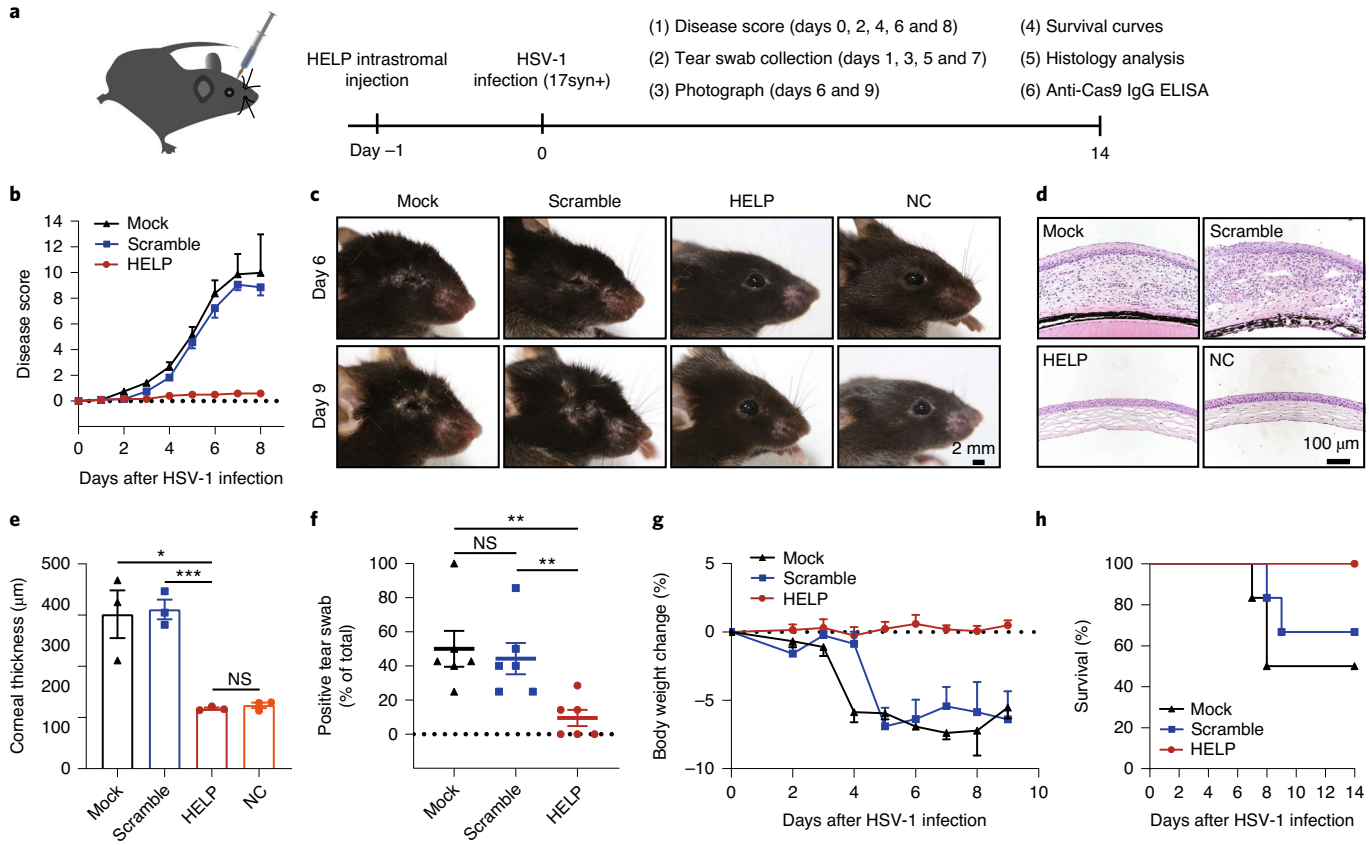

Fig. 3 | HELP suppresses HSV-1-associated disease pathologies in the prevention model. a, Flowchart for evaluating the antiviral effects of HELP in vivo. p24 HELP (100 ng), scramble mLP or 2 μl PBS (mock) was injected into corneas. After 24 h, the mice were infected with HSV-1 17syn+ (2×10^6 p.f.u. per eye). **b**, Ocular disease scores (0 to 4, with 4 being severe) in mice; $n=6$ mice. **c**, Photographs of the right eyes of mice from the different treatment groups 6 d.p.i. and 9 d.p.i. Each image is representative of three mice in one experiment. NC, non-treated control. **d**, Corneal histology of eyes 14 d.p.i. Each image is representative of three mice in two independent experiments. **e**, Thickness of the cornea as assessed by histology; $n=3$ mice. HELP versus mock and scramble, $P=0.0168$ and 0.0006, respectively. **f**, Secreted HSV-1 as assessed by eye swabs. Tear swabs from each mouse were collected at 1, 3, 5 and 7 d.p.i. The percentage of HSV-1-positive swabs was recorded; $n=6$ mice. Mock versus HELP, $P=0.0056$; scramble versus HELP, $P=0.0072$. **g**, Change in body weight; $n=6$ mice. **h**, Kaplan–Meier survival curves; $n=6$ mice. Data and error bars represent mean ± s.e.m.; unpaired two-tailed Student's *t* tests; NS, not significant.

Importantly, mice treated with HELP did not show any disease progression ($n=6$ mice), while the mock-treated and scrambled gRNA-treated eyes developed severe signs of ocular infection (Fig. 3b,c). Next, we performed histological staining to examine the pathology of the eye. The mock- and scrambled gRNA-treated eyes presented with irregular stromal matrix and increased corneal thickness, typical signs of acute infection (Fig. 3d,e). We further found that HSV-1 infection in the corneas induced a significant type I IFN response, while HELP transduction did not elicit such a response (Supplementary Fig. 11). Clinical HSK is the result of excessive virus-induced corneal inflammation mediated by the infiltration of inflammatory cells, including T cells (both $CD4^+$ and $CD8^+$), polymorphonuclear leukocytes and macrophages[34,35]. Indeed, HSV-1 infection provoked corneal expression of the inflammatory molecules IL-6, CCL2 and CXCL10, which was blocked after HELP treatment (Supplementary Fig. 12). Using immunohistochemistry, we showed that HSV-1 infection led to infiltration of $CD4^+$ and $CD8^+$ T cells in the corneal stroma for the mock- and scrambled control-treated groups, but HELP treatment prevented T cell infiltration (Supplementary Fig. 13). Additionally, we stained corneal sections for two additional markers, CD11b and F4/80, to visualize myeloid-derived cells and macrophages, respectively. We observed $CD11b^+$ and $F4/80^+$ cells in non-therapeutic groups in contrast to mice treated with HELP and non-infected controls (Supplementary Fig. 13). We also noted that PD-L1 was upregulated in the epithelium and stroma of untreated mice after HSV-1 infection, consistent with previous observations (Supplementary Fig. 13; ref. [36]). Increased local PD-L1 expression may inhibit viral clearance by immune cells, highlighting the importance of direct DNA degradation by CRISPR. To assess the presence of secreted virus, the viral titer of eye swabs was determined every other day after infection. HELP treatments significantly reduced viral presence in the eyes (Fig. 3f). In addition, body weights were recorded every other day. No loss of body weight was observed for HELP-treated mice, while it was evident for the mock- and scrambled control-treated mice (Fig. 3g). Notably, all mice survived in the HELP-treated groups and no relapse of HSK for the HELP-treated mice was found during the 3-month follow-up (Fig. 3h and Supplementary Fig. 14).

Eye health after HELP treatment in the prevention model. Subsequently, we thoroughly analyzed corneal health using clinically relevant indices (Fig. 4a). To determine lesion formation, we assessed the epithelial layers of corneas using sodium fluorescein, which stains damaged epithelial cells. We found that HELP-treated corneas were significantly protected from HSV-1 infection (Fig. 4b). As reduced tear production has been shown in HSK, we assessed

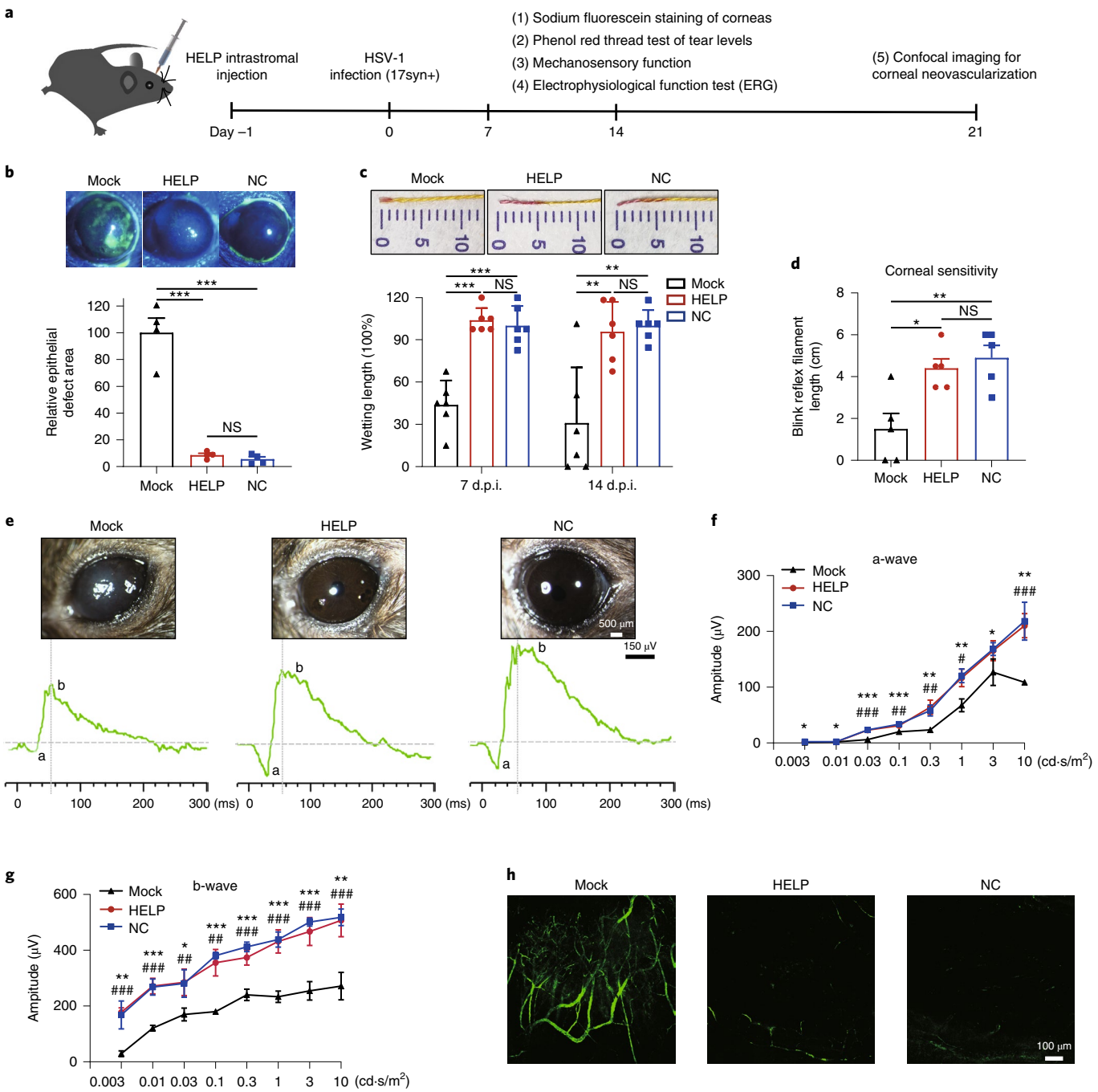

Fig. 4 | Eye health after HELP treatment in the prevention model. a, Flowchart for evaluating eye health in the prevention model. p24 HELP (100 ng) or 2 μl PBS (mock) was delivered into corneas 24 h before the mice were infected with HSV-1 17syn+ (2×10^6 p.f.u. per eye). **b**, Sodium fluorescein staining of mouse corneas. The area with defects in HELP-treated and NC mice was normalized to that in mock-treated mice; $n=4$ mice. Mock versus HELP and NC, $P=0.0002$ and 0.0001, respectively. **c**, Phenol red thread test of the wettability of tear fluid; $n=6$ mice. Mock versus HELP, $P<0.0001$ at 7 d.p.i. and $P=0.0054$ at 14 d.p.i.; mock versus NC, $P=0.0001$ at 7 d.p.i. and $P=0.0021$ at 14 d.p.i. Wettability indicates the ability of eyes to produce tears. Upon contact with tears, the color of the phenol red thread changes from light yellow to deep red. The length of the red color directly corresponds to the tearing ability of the eyes. **d**, Measurement of the mechanosensory function of the corneas by esthesiometer; $n=5$ mice. Mock versus HELP, $P=0.0104$; mock versus NC, $P=0.0074$. **e**–**g**, Change in ERG amplitudes of treated eyes. **e**, Corneal graphs and traces of the a-waves and b-waves. **f**,**g**, Quantitative analysis of a-wave (**f**) and b-wave (**g**) amplitude; $n=5$ mice. In **f**, NC versus mock (*), $P=0.02$, 0.01, 0.00002, 0.0006, 0.0026, 0.0036, 0.03 and 0.002; HELP versus mock (#), $P=0.0002$, 0.0092, 0.0018, 0.0114 and 0.0005; for increasing values of cd·s/m². In **g**, NC versus mock (*), $P=0.0040$, 0.0003, 0.0200, 0.00001, 0.00001, 0.0001, 0.0001 and 0.0015; HELP versus mock (#), $P=0.0001$, 0.0002, 0.0047, 0.0011, 0.0007, 0.0004, 0.0005 and 0.0005; for increasing values of cd·s/m². **h**, Confocal microscopy imaging of neovascularization in the corneas. Data and error bars represent mean ± s.e.m.; unpaired two-tailed Student's *t* tests; NS, not significant. Each image is representative of three mice in one experiment (**b**,**e**,**h**).

the tear secretion levels of mice using the phenol red thread test. We found that HELP treatment significantly protected the infected corneas from desiccation (Fig. 4c). HSV-1 infection often causes denervation of the cornea with a substantial loss of sensory fibers. Next, we measured the mechanosensory function of the corneas using an esthesiometer and showed that the sensory function of

corneas was preserved (Fig. 4d). We further determined the effects of HELP on visual function by full-field electroretinography (ERG). Waveforms were evaluated for negative a-wave (photoreceptor responses) and positive b-wave (cone and rod system responses) amplitudes (Fig. 4e). As shown in Fig. 4f,g, the amplitudes of a-waves and b-waves were significantly reduced in mock-treated eyes (a-waves, $23.36 \pm 2.4\,\mu V$ versus $58.11 \pm 10\,\mu V$, $P < 0.01$; b-waves, $240.12 \pm 20.49\,\mu V$ versus $412.3 \pm 17.38\,\mu V$, $P < 0.001$; $n = 5$ mice) compared to non-infected control eyes (NC) with a flash stimulus at $3\,cd{\cdot}s/m^2$ (mixed cone–rod response). The effect on the a-wave and b-wave amplitudes after HELP application was significantly larger with a flash stimulus of $3\,cd{\cdot}s/m^2$ than for mock-treated eyes (a-waves, $64.33 \pm 13.02\,\mu V$ versus $23.36 \pm 2.4\,\mu V$, $P < 0.01$; b-waves, $374.44 \pm 27.5\,\mu V$ versus $240.12 \pm 20.49\,\mu V$, $P < 0.001$; $n = 5$ mice). These results confirm that experimental HSK in mice leads to serious deficits in visual function, likely due to the reduced transparency of corneas and the lower intensity of the light stimulus received by the retina and not as a result of direct retinal damage (Supplementary Fig. 15). Visual deficits could be prevented by the administration of HELP. Neovascularization is a hallmark of HSK[37]. We therefore assessed the degree of corneal neovascularization by whole-mount fluorescein isothiocyanate (FITC)-conjugated dextran (FITC–dextran) staining (Fig. 4h). Indeed, HSV-1 infection induced neovascularization in corneas, which was inhibited by HELP treatment.

Additionally, we examined whether intrastromal injection of HELP induces Cas9-specific IgG in the bloodstream. We did not observe significantly higher Cas9-specific IgG in either HELP- or scrambled control-treated mice than in mock-treated mice ($n = 5$ mice; non-significant, Student's t tests). In contrast, when HELP was injected via the footpad route, it provoked significantly higher levels of anti-Cas9 IgG in the sera ($n = 3$ mice; $P < 0.001$, Student's t tests; Supplementary Fig. 16). Interestingly, ocular infection with HSV-1 induced high titers of anti-HSV-1 neutralizing antibodies, which were absent after HELP treatment (Supplementary Fig. 17). Taken together, these results suggest that the administration of HELP significantly reduced the manifestation of disease severity during ocular HSV-1 infection.

HELP cures HSK in therapeutic and recurrent models. To better mimic the therapeutic process of HSK, we administered HELP after HSV infection and evaluated the therapeutic efficacy. We initially inoculated mice with HSV-1 at a dose of 2×10^6 p.f.u. per eye and treated the mice with HELP or ACV, which was used as a positive control (Fig. 5a). We found that both ACV and HELP treatment inhibited lesions in the eyelids (Fig. 5b). Both ACV and HELP significantly reduced the secretion of infectious HSV-1 in tear swabs (Fig. 5c,d). Interestingly, only HELP significantly reduced the levels of infectious HSV-1 in the eyes, suggesting the unique advantage of CRISPR in eliminating viruses (Fig. 5e). While all mice from the mock-treated group died, both HELP and ACV treatment significantly augmented survival rates, with HELP showing superior effects compared to ACV (Fig. 5f). Next, we lowered the dose of HSV-1 to 5×10^4 p.f.u. per eye (Fig. 5g). In addition, we injected HELP 1 d instead of 2 d after HSV-1 infection (Fig. 5g). The corneas of mock-treated animals developed symptoms of HSK 14 d after infection, while both ACV and HELP treatment prevented disease progression (Fig. 5h). Next, we evaluated the mechanosensory function of the corneas and found that it was maintained for both ACV and HELP but not for mock treatment (Fig. 5i). Additionally, we performed confocal microscopy analyses of the cornea by staining sensory fibers and damaged collagen fibers, thus evaluating corneal health. We found loss of β-III-tubulin and increased appearance of collagen-binding peptides in mock-treated mice, which were absent in both the ACV and HELP treatment groups (Fig. 5j,k). Furthermore, we assessed HSV-1 distribution in the corneas and TG. We found that both ACV and HELP blocked HSV-1 replication in the corneas, with HELP showing superior efficiency (Fig. 5l). Strikingly, while ACV failed to modulate the HSV-1 reservoir in the TG, HELP diminished the HSV-1 viral load to an almost undetectable level in the TG, likely via retrograde transport (Fig. 5m).

To strengthen the notion that HELP can modulate the HSV reservoir, we adopted a recurrent HSK model in which eyes were infected with HSV-1 to establish latency before HELP treatment (Fig. 5n). We reactivated disease in mice that survived acute HSV-1 infection by UV-B irradiation of the eyes 60 d after HSV-1 inoculation. We then treated eyes with HELP by intrastromal injection and quantified HSV-1 genome 7 d later. We found that HELP significantly decreased viral load in the eyes, which migrated from the TG by anterograde transport (Fig. 5o). In agreement with Fig. 5m, we found a significantly reduced level of HSV-1 in the TG (Fig. 5p).

HELP eliminates HSV-1 in tissue culture of human corneas. Having established the therapeutic efficacy of HELP in mouse models, we sought to investigate the antiviral potential of HELP in human corneas (Fig. 6a). One human cornea was evenly divided into two halves and injected with either 15 µl HELP (equal to 1.5 µg of p24) or PBS for confocal imaging. We found that HELP was evenly spread in the stroma and potently inhibited HSV-1 (17syn+) replication, as evidenced by reduced VP5 expression compared to mock-treated control cornea (Fig. 6b,c). Using the cornea from another donor, we found that HELP treatment significantly diminished both the amount of HSV-1 genome and viral titer (Fig. 6d,e). Additionally, we found that VP5 protein was hardly detectable by western blotting after HELP treatment (Fig. 6f). To examine whether HELP causes off-target effects in the human genome, we performed whole-genome sequencing (WGS) on a human cornea that was evenly divided for HELP and PBS injection. We analyzed the single-nucleotide variants (SNVs) and indels at an average depth of 51- and 45-fold for HELP and mock-treated cornea, respectively, including coding, splicing, up- and downstream, noncoding RNA, 5′- and 3′-UTR, intronic and intergenic regions. In total, 4,123,284 SNVs and 1,328,314 indels were detected

Fig. 5 | HELP cures HSK in the therapeutic and recurrent models. a, Flowchart for evaluating the antiviral effects of HELP in the HSK therapeutic model. Mice were infected with HSV-1 17syn+ (2×10^6 p.f.u. per eye). After 48 h, 100 ng of p24 HELP or 2 µl PBS (mock) was administrated. ACV was added topically to both eyes every day for 5 d. **b**, Photographs of the eyes of mice from the different treatment groups. **c**,**d**, Infectious units in tear swabs at 3 d.p.i. (**c**) and 5 d.p.i. (**d**); $n = 7$ mice. In **c**, mock versus HELP, $P = 0.0083$; ACV versus HELP, $P = 0.0060$. In **d**, mock versus ACV, $P = 0.0031$; mock versus HELP, $P = 0.0431$. **e**, Plaque assay for HSV-1 in the eyes; $n = 7$ mice. Mock versus HELP, $P = 0.0197$; ACV versus HELP, $P = 0.0360$. **f**, Kaplan–Meier survival curves; $n = 6$ mice. Mock versus HELP and ACV, $P = 0.0076$ and 0.0297, respectively. **g**, Flowchart for evaluating the antiviral effects of HELP in the HSK therapeutic model. HSV-1 was used at 5×10^4 p.f.u. per eye. **h**, Photographs of the eyes of mice from the different treatment groups. **i**, Measurement of the mechanosensory function of the corneas by esthesiometer; $n = 4$ mice. Mock versus HELP and ACV, $P = 0.0127$ and 0.0349, respectively. **j**,**k**, Confocal images of sensory fibers (**j**) and damaged collagen (**k**) in corneas. **l**,**m**, Confocal images of HSV-1 (VP5) in the corneas (**l**) and HELP (anti-GFP) in the TG (**m**). **n**, Flowchart for evaluating antiviral activity using a recurrent HSK model. Mice were infected with HSV-1 17syn+ (2×10^5 p.f.u. per eye). **o**,**p**, Viral load in the eyes (**o**) and TG (**p**) as detected by qPCR; $n = 4$ mice; $P = 0.0004$ (**o**) and $P = 0.0179$ (**p**). Data and error bars represent mean ± s.e.m.; unpaired two-tailed Student's t tests; NS, not significant. Each image is representative of four (**b**,**h**) or two (**j**–**m**) mice in one experiment.

in HELP-treated cornea and 3,726,678 SNVs and 981,253 indels were detected in mock-treated cornea (Fig. 6g and Supplementary Figs. 18 and 19). We then filtered the SNVs and indels using 707 Cas-OFFinder-predicted off-target sites and the WGS sequence for mock-treated cornea[38]. In total, we found 31 SNV and 7 indel mutations (Supplementary Tables 1 and 2), but none of them were located in coding regions, indicating no functional off-target sites in HELP-treated human corneas (Fig. 6h).

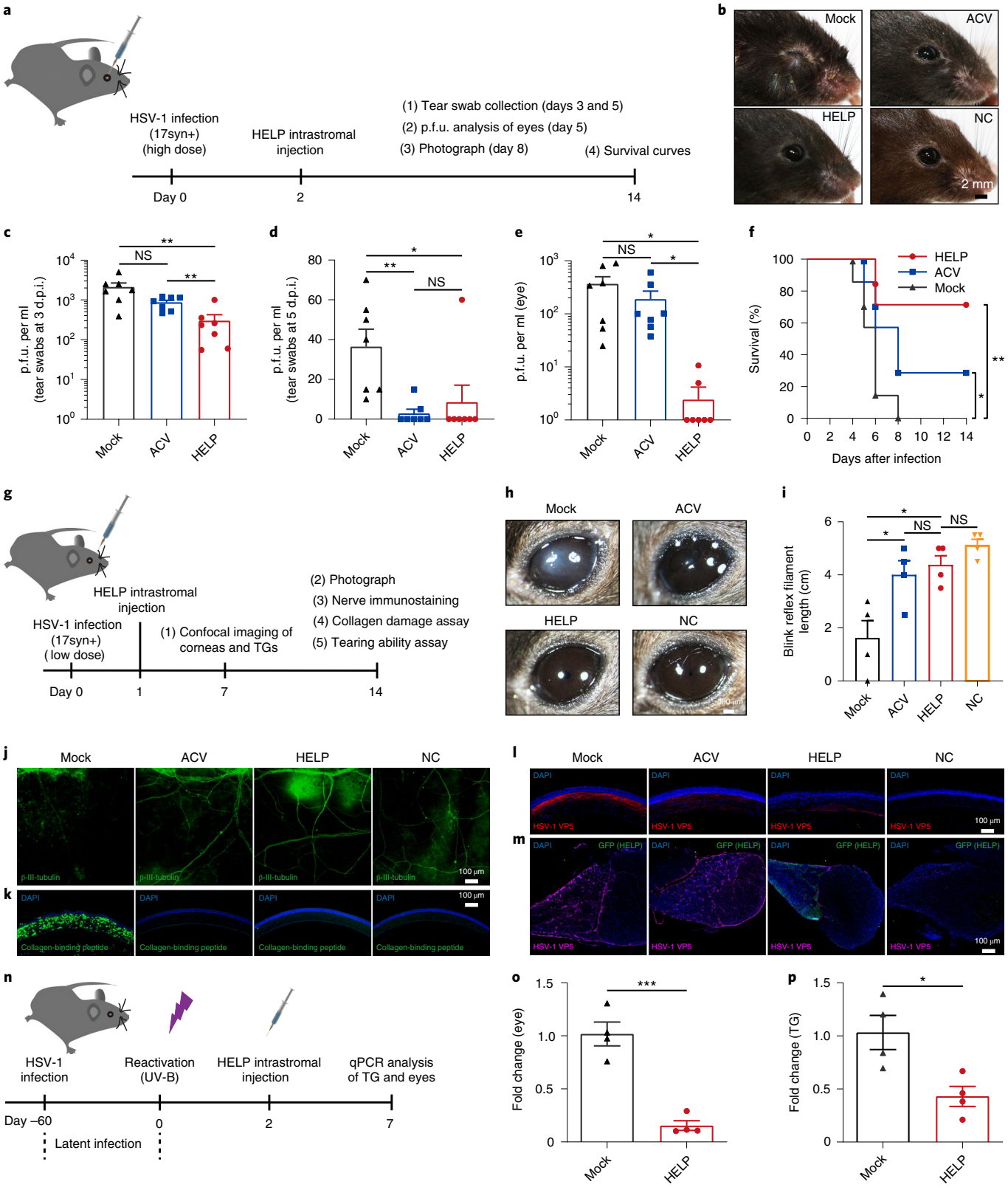

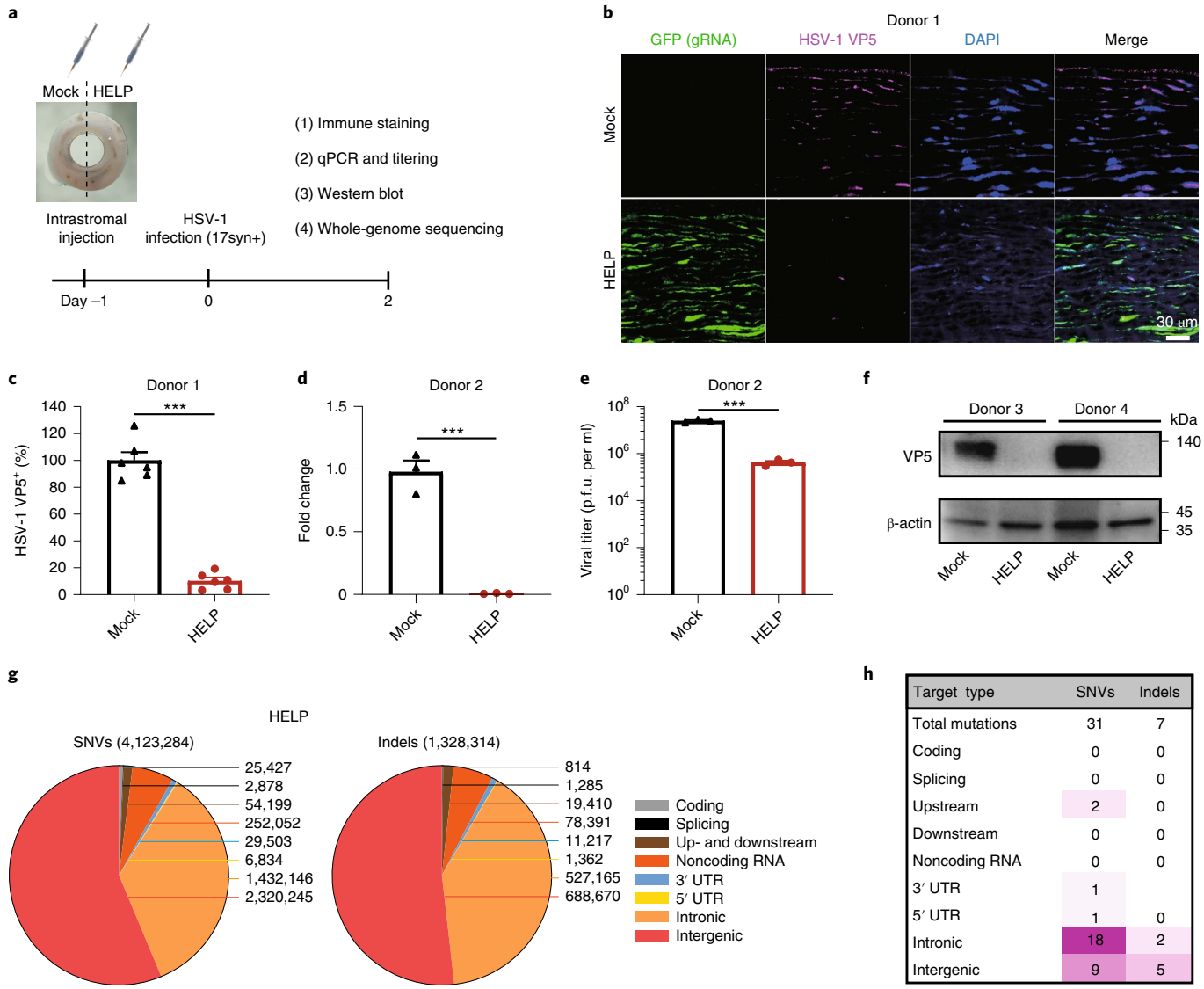

h

Target type	SNVs	Indels
Total mutations	31	7
Coding	0	0
Splicing	0	0
Upstream	2	0
Downstream	0	0
Noncoding RNA	0	0
3′ UTR	1	
5′ UTR	1	0
Intronic	18	2
Intergenic	9	5

Fig. 6 | HELP eliminates HSV-1 in tissue culture of human corneas. a, Flowchart for evaluating the antiviral effects of HELP in human corneas. p24 HELP (1.5 μg) or 15 μl PBS (mock) was injected into the corresponding punches derived from the same human cornea. After 24 h, the corneal punches were infected with HSV-1 17syn+ (2×10^6 p.f.u. per piece). **b**, Confocal analysis of the distribution of HSV-1 and HELP in human cornea. GFP is indicative of the presence of HELP and VP5 is indicative of the presence of HSV-1. **c**, Percentage of VP5$^+$ cells presented in **b**. Data are shown as the percentage of mock-treated tissues; $n=6$ biologically independent samples; $P<0.0001$. **d**, qPCR analysis of HSV-1 genome (fold change); $n=3$ biologically independent samples; $P=0.0005$. **e**, Titering of supernatants from human corneal cultures; $n=3$ biologically independent samples; $P=0.0003$. **f**, Western blot analysis of VP5 protein expression. The experiment was repeated twice with similar results. **g**, Identification of SNV and indel mutations in a HELP-treated corneal punch at the WGS level. Valid sequencing data were aligned to human genome version 19 (hg19). **h**, Summary of unique SNV and indel mutations. Data and error bars represent mean ± s.e.m.; unpaired two-tailed Student's *t* tests.

Discussion

In this study, we show that transient gene editing via mRNA-based CRISPR delivery is sufficient to achieve therapeutic efficacy against HSK in vivo and blocks HSV-1 replication in human corneas. Modulating the viral reservoir is essential to prevent HSK from recurrence. Further, our study provides evidence of HSV elimination in the reservoir by HELP via retrograde transport from the cornea to the TG.

The administration of HELP was through intrastromal delivery, which has been frequently used in clinical practice to deliver bevacizumab to the corneal stroma of patients with HSK to prevent corneal neovascularization[39,40]. In addition, intrastromal injection of antibiotics is a routine procedure to treat patients with fungal keratitis[41,42]. Using a set of evaluation methods, including sodium fluorescein staining, a phenol red thread test, an esthesiometer, ERG and FITC–dextran, β-III-tubulin and peptide staining, we showed healthy corneal status after CRISPR therapy, suggesting that the intrastromal injection of HELP is practical for clinical translation.

HSK is thought to be the result of HSV-1-induced corneal infiltration of a cocktail of inflammatory cells, consisting of T cells (both CD4$^+$ and CD8$^+$), macrophages and polymorphonuclear leukocytes. Corneas removed from patients requiring corneal transplants due to HSK contained both CD4$^+$ and CD8$^+$ T cells[43,44]. Consistent with this, our study also showed infiltration of both CD4$^+$ and CD8$^+$ T cells in the corneas of HSV-infected mice. Moreover, we also found infiltration of myeloid-derived cells and macrophages

in HSV-1-infected corneas (Supplementary Fig. 13). Notably, the infiltration of inflammatory cells was prevented after HELP administration.

In humans, HSK often develops after virus replication can be detected and may develop after most of the replicating virus is cleared[7]. Asymptomatic virus shedding has been reported in tears of healthy individuals, although it is relatively rare[45]. As HELP treatment represents an antiviral therapy, the optimal efficacy of HELP treatment may be linked to the time point of administration, which has to be investigated by clinical testing. From a clinical perspective, HELP may first be applied to patients with acute corneal perforation or corneal graft failure due to the recurrence of virus in combination with keratoplasty. Given the safety and efficacy this treatment shows in the most serious instances of HSK, HELP may also be extended to early-stage HSK as a first-line choice to cure or prevent the recurrence of HSK by eliminating virus in the corneas and TG.

The HELP used in the current study are coated by VSV-G envelope protein. Lentiviral vector pseudotyped by VSV-G is capable of retrograde transport potentially mediated by cytoplasmic dynein, as has been shown previously[46,47]. Our study has demonstrated the possibility to reduce HSV-1 levels in the TG; however, the efficiency may further be enhanced by coating HELP with derivatives of rabies virus glycoprotein[46,48].

While our manuscript was under revision, Aubert et al. reported that AAV delivery of meganucleases was also capable of modulating latent HSV-1 in vivo[26]. The study, however, largely focused on analysis of HSV-1 genomes and did not include a disease model. Therefore, it is difficult to predict the therapeutic benefits. Notably, the study detected only low levels of gene editing of HSV with CRISPR, likely due to the large size of Cas9 and low expression of Cas9 and gRNA from the single-stranded AAV in vivo[26]. In contrast, HELP is able to overcome the size limitation of AAV and co-package both SpCas9 and gRNA to efficiently eliminate HSV genomes in vivo, decreasing the amount of viral genome by 1 to 2 log more than meganucleases. Importantly, HELP is mRNA based and promoterless for Cas9. In contrast, AAV constructs will likely persist for a long time in non-dividing neurons and require a strong promoter for efficient nuclease expression; they are therefore accompanied by long-term safety risks from a clinical perspective.

In conclusion, the efficacy and safety profile of HELP shown in our study strongly supports further clinical testing of these lentiviral particles targeting HSV-1 by CRISPR. Additionally, because the gRNAs of HELP target the genome of the virus instead of the human genome, this may accelerate clinical translation. Our study may also facilitate the development of CRISPR therapeutics targeting other viruses such as human papillomavirus (HPV) or inherited diseases.

Online content

Any methods, additional references, Nature Research reporting summaries, source data, extended data, supplementary information, acknowledgements, peer review information; details of author contributions and competing interests; and statements of data and code availability are available at https://doi.org/10.1038/s41587-020-00781-8.

Received: 21 August 2020; Accepted: 19 November 2020;
Published online: 11 January 2021

References

1. Liesegang, T. J. Herpes simplex virus epidemiology and ocular importance. *Cornea* **20**, 1–13 (2001).
2. Paludan, S. R., Bowie, A. G., Horan, K. A. & Fitzgerald, K. A. Recognition of herpesviruses by the innate immune system. *Nat. Rev. Immunol.* **11**, 143–154 (2011).
3. Bradshaw, M. J. & Venkatesan, A. Herpes simplex virus-1 encephalitis in adults: pathophysiology, diagnosis, and management. *Neurotherapeutics* **13**, 493–508 (2016).
4. Farooq, A. V. & Shukla, D. Herpes simplex epithelial and stromal keratitis: an epidemiologic update. *Surv. Ophthalmol.* **57**, 448–462 (2012).
5. Crumpacker, C. S. & Schaffer, P. A. New anti-HSV therapeutics target the helicase–primase complex. *Nat. Med.* **8**, 327–328 (2002).
6. Remeijer, L. et al. Prevalence and clinical consequences of herpes simplex virus type 1 DNA in human cornea tissues. *J. Infect. Dis.* **200**, 11–19 (2009).
7. Wang, L., Wang, R., Xu, C. & Zhou, H. Pathogenesis of herpes stromal keratitis: immune inflammatory response mediated by inflammatory regulators. *Front. Immunol.* **11**, 766 (2020).
8. Awasthi, S. et al. Nucleoside-modified mRNA encoding HSV-2 glycoproteins C, D, and E prevents clinical and subclinical genital herpes. *Sci. Immunol.* **4**, eaaw7083 (2019).
9. Bolland, S. & Pierce, S. K. Ups and downs in the search for a herpes simplex virus vaccine. *eLife* **4**, e06883 (2015).
10. Vadlapudi, A. D., Vadlapatla, R. K. & Mitra, A. K. Update on emerging antivirals for the management of herpes simplex virus infections: a patenting perspective. *Recent Pat. Antiinfect. Drug Discov.* **8**, 55–67 (2013).
11. Jiang, Y. C., Feng, H., Lin, Y. C. & Guo, X. R. New strategies against drug resistance to herpes simplex virus. *Int. J. Oral Sci.* **8**, 1–6 (2016).
12. Schaeffer, H. J. et al. 9-(2-hydroxyethoxymethyl) guanine activity against viruses of the herpes group. *Nature* **272**, 583–585 (1978).
13. Koganti, R., Yadavalli, T. & Shukla, D. Current and emerging therapies for ocular herpes simplex virus type-1 infections. *Microorganisms* **7**, 429 (2019).
14. Crute, J. J. et al. Herpes simplex virus helicase–primase inhibitors are active in animal models of human disease. *Nat. Med.* **8**, 386–391 (2002).
15. Kleymann, G. et al. New helicase–primase inhibitors as drug candidates for the treatment of herpes simplex disease. *Nat. Med.* **8**, 392–398 (2002).
16. Jaishankar, D. et al. An off-target effect of BX795 blocks herpes simplex virus type 1 infection of the eye. *Sci. Transl. Med.* **10**, eaan5861 (2018).
17. Nelson, C. E. et al. Long-term evaluation of AAV-CRISPR genome editing for Duchenne muscular dystrophy. *Nat. Med.* **25**, 427–432 (2019).
18. Maeder, M. L. et al. Development of a gene-editing approach to restore vision loss in Leber congenital amaurosis type 10. *Nat. Med.* **25**, 229–233 (2019).
19. Beyret, E. et al. Single-dose CRISPR–Cas9 therapy extends lifespan of mice with Hutchinson–Gilford progeria syndrome. *Nat. Med.* **25**, 419–422 (2019).
20. Santiago-Fernandez, O. et al. Development of a CRISPR/Cas9-based therapy for Hutchinson–Gilford progeria syndrome. *Nat. Med.* **25**, 423–426 (2019).
21. Lee, B. et al. Nanoparticle delivery of CRISPR into the brain rescues a mouse model of fragile X syndrome from exaggerated repetitive behaviours. *Nat. Biomed. Eng.* **2**, 497–507 (2018).
22. Gao, X. et al. Treatment of autosomal dominant hearing loss by in vivo delivery of genome editing agents. *Nature* **553**, 217–221 (2018).
23. Dash, P. K. et al. Sequential LASER ART and CRISPR treatments eliminate HIV-1 in a subset of infected humanized mice. *Nat. Commun.* **10**, 2753 (2019).
24. de Buhr, H. & Lebbink, R. J. Harnessing CRISPR to combat human viral infections. *Curr. Opin. Immunol.* **54**, 123–129 (2018).
25. Aubert, M. et al. In vivo disruption of latent HSV by designer endonuclease therapy. *JCI Insight* **1**, e88468 (2016).
26. Aubert, M. et al. Gene editing and elimination of latent herpes simplex virus in vivo. *Nat. Commun.* **11**, 4148 (2020).
27. van Diemen, F. R. et al. CRISPR/Cas9-mediated genome editing of herpesviruses limits productive and latent infections. *PLoS Pathog.* **12**, e1005701 (2016).
28. Oh, H. S. et al. Herpesviral lytic gene functions render the viral genome susceptible to novel editing by CRISPR/Cas9. *eLife* **8**, e51662 (2019).
29. Weerasooriya, S., DiScipio, K. A., Darwish, A. S., Bai, P. & Weller, S. K. Herpes simplex virus 1 ICP8 mutant lacking annealing activity is deficient for viral DNA replication. *Proc. Natl Acad. Sci. USA* **116**, 1033–1042 (2019).
30. Weller, S. K. & Coen, D. M. Herpes simplex viruses: mechanisms of DNA replication. *Cold Spring Harb. Perspect. Biol.* **4**, a013011 (2012).
31. Reinert, L. S. et al. Sensing of HSV-1 by the cGAS–STING pathway in microglia orchestrates antiviral defence in the CNS. *Nat. Commun.* **7**, 13348 (2016).
32. Herpetic Eye Disease Study Group. Oral acyclovir for herpes simplex virus eye disease: effect on prevention of epithelial keratitis and stromal keratitis. *Arch. Ophthalmol.* **118**, 1030–1036 (2000).
33. Kennedy, D. P. et al. Ocular herpes simplex virus type 1: is the cornea a reservoir for viral latency or a fast pit stop? *Cornea* **30**, 251–259 (2011).
34. Newell, C. K., Martin, S., Sendele, D., Mercadal, C. M. & Rouse, B. T. Herpes simplex virus-induced stromal keratitis: role of T-lymphocyte subsets in immunopathology. *J. Virol.* **63**, 769–775 (1989).

35. Stuart, P. M., Summers, B., Morris, J. E., Morrison, L. A. & Leib, D. A. CD8+ T cells control corneal disease following ocular infection with herpes simplex virus type 1. *J. Gen. Virol.* **85**, 2055–2063 (2004).
36. Jeon, S., Rowe, A. M., Carroll, K. L., Harvey, S. A. K. & Hendricks, R. L. PD-L1/B7-H1 inhibits viral clearance by macrophages in HSV-1-infected corneas. *J. Immunol.* **200**, 3711–3719 (2018).
37. Biswas, P. S. & Rouse, B. T. Early events in HSV keratitis—setting the stage for a blinding disease. *Microbes Infect.* **7**, 799–810 (2005).
38. Bae, S., Park, J. & Kim, J.-S. Cas-OFFinder: a fast and versatile algorithm that searches for potential off-target sites of Cas9 RNA-guided endonucleases. *Bioinformatics* **30**, 1473–1475 (2014).
39. Sarah, B., Ibtissam, H., Mohammed, B., Hasna, S. & Abdeljalil, M. Intrastromal injection of bevacizumab in the management of corneal neovascularization: about 25 eyes. *J. Ophthalmol.* **2016**, 6084270 (2016).
40. Berrozpe-Villabona, C. et al. Intrastromal bevacizumab injection for corneal neovascularization in herpetic stromal keratitis. *J. Fr. Ophtalmol.* **38**, 776–777 (2015).
41. Sharma, N. et al. Management algorithm for fungal keratitis: the TST (topical, systemic, and targeted therapy) protocol. *Cornea* **38**, 141–145 (2019).
42. Narayana, S. et al. Mycotic antimicrobial localized injection: a randomized clinical trial evaluating intrastromal injection of voriconazole. *Ophthalmology* **126**, 1084–1089 (2019).
43. Koelle, D. M. et al. Tegument-specific, virus-reactive CD4 T cells localize to the cornea in herpes simplex virus interstitial keratitis in humans. *J. Virol.* **74**, 10930–10938 (2000).
44. Maertzdorf, J., Verjans, G. M., Remeijer, L., van der Kooi, A. & Osterhaus, A. D. Restricted T cell receptor β-chain variable region protein use by cornea-derived CD4+ and CD8+ herpes simplex virus-specific T cells in patients with herpetic stromal keratitis. *J. Infect. Dis.* **187**, 550–558 (2003).
45. Okinaga, S. Shedding of herpes simplex virus type 1 into tears and saliva in healthy Japanese adults. *Kurume Med. J.* **47**, 273–277 (2000).
46. Kobayashi, K. et al. Pseudotyped lentiviral vectors for retrograde gene delivery into target brain regions. *Front. Neuroanat.* **11**, 65 (2017).
47. Arriagada, G. Retroviruses and microtubule-associated motor proteins. *Cell. Microbiol.* **19**, e12759 (2017).
48. Kato, S. et al. Enhancement of the transduction efficiency of a lentiviral vector for neuron-specific retrograde gene delivery through the point mutation of fusion glycoprotein type E. *J. Neurosci. Methods* **311**, 147–155 (2019).

Methods

Cell cultures and HSV-1 propagation. Vero, 293T, HaCaT and HaCaT *IFNAR2*-knockout cells were cultured in DMEM (Gibco). THP-1 cells were cultured in RPMI 1640 (Gibco). DMEM and RPMI 1640 media were supplemented with 10% FBS (Gibco) and 1% penicillin/streptomycin (P/S; Thermo Fisher Scientific). All cell lines used were obtained from the laboratory of S. R. Paludan and not authenticated in our laboratory. None of the cell lines were listed in the database of commonly misidentified cell lines maintained by the International Cell Line Authentication Committee. Primary mouse corneal stromal cells were digested from corneal stromal tissues and maintained in MEM (Gibco) supplemented with 1% P/S and 10% FBS. Human cornea tissues were maintained in MEM (Gibco) supplemented with 1% P/S and 10% FBS. All cells were cultured at 37 °C and 5% CO_2. HSV-1 strains, including 17syn+, McKrae, F and HSV-1–GFP (HSV-1 KOS strain expressing GFP driven by the CMV promoter)[31], were propagated and titered in Vero cells. Only 17syn+ was used for in vivo study. All cell lines tested negative for mycoplasma contamination.

Production of mRNA-carrying lentiviral particles. 293T cells were seeded in 15-cm dishes at a density of 1×10^7 cells per dish 24 h before calcium phosphate transfection. Twenty-four hours after transfection, the medium was refreshed and the supernatants were harvested 48 h and 72 h after transfection before passing through a 0.22-μm filter (Millipore) and ultracentrifugation at 25,000 r.p.m. at 4 °C for 2 h. Pellets were resuspended in PBS and stored at −80 °C. To produce 'all-in-one' mLPs, 293T cells were transfected with 9.07 μg pMD.2G, 7.26 μg pRSV-Rev, 15.74 μg pMDlg/pRRE-D64V, 15.74 μg pMS2M-PH-gagpol-D64V, 31.46 μg pCMV-Cas9-6XMS2 and 31.46 μg pLV-egfp-U3-osp-gRNA with corresponding gRNA sequence. To produce HELP, pLV-U6-UL29-egfp-U3-UL8 was used as the gRNA-producing plasmid. To produce the non-GFP version of HELP, pLV-U6-UL29-U3-UL8 was used. The plasmids are deposited in Addgene.

HSV-1 plaque assay. HSV-1 plaque assays were performed in triplicate for each biological sample. Vero cells (1.5×10^5) were seeded in a 12-well plate in complete DMEM and infected the following day with various dilutions of HSV stocks or culture supernatants. Two hours after infection, cells were overlaid with 1% agarose (Sangon) solution. After incubation for 3 d, cells were fixed with 4% formaldehyde and stained using 1% crystal violet solution at room temperature for 2 h. After three washes with PBS, plates were allowed to dry and the number of plaques was counted. Viral titers were calculated as p.f.u. per ml.

Infection and transduction of cells. For 293T, HaCaT, HaCaT *IFNAR2*-knockout, THP-1 and primary mouse corneal stromal cells, 4×10^4 cells were seeded in a 48-well plate and transduced with 400 ng of mLPs on the following day. The medium was refreshed 12 h post-infection (h.p.i.). After a 24-h transduction, cells were infected with HSV-1–GFP at an MOI of 1. The cells and supernatants were harvested at 24 and 48 h.p.i. for flow cytometry and plaque assays, respectively. To determine the cleavage activity for HSV-1 genomes, DNA was isolated from cell lysates using the viral DNA extraction kit (TaKaRa) and sequenced by Sanger sequencing and TIDE 2.0.1 analysis. The sequences for the primers used are shown in Supplementary Table 3.

Flow cytometry analysis. Primary mouse corneal stromal cells were seeded at a density of 4×10^4 cells per well on day 1 and were transduced with *UL29*/*UL8* co-targeting HELP or scrambled control (non-GFP version) on day 2. The cells were then infected with HSV-1–GFP on day 3. GFP signals were determined by flow cytometry (BD LSRFortessa, BD Biosciences). On days 4 and 5, data were collected by BD FACSDiva 7 and analyzed by FlowJo 7.6 for the percentage of GFP^+ cells and mean fluorescence intensity. Gating strategies are shown in Supplementary Fig. 20.

ELISA. The p24 protein of mLP was measured using an HIV p24 ELISA according to the manufacturer's instructions (Beijing Biodragon Immunotechnologies). To detect the mouse humoral IgG immune response to Cas9, an IgG mouse ELISA kit (Abcam) was used following the manufacturer's protocol with a few modifications. Recombinant Cas9 protein (0.25 μg; Novoprotein) was suspended in PBS and used to coat 96-well ELISA plates, which were incubated at 4 °C for 12 h and then washed three times using 1× wash buffer. Plates were blocked with 2% BSA blocking solution for 2 h at room temperature and then washed three times. Serum samples were added to each well. The remaining steps were performed according to the manufacturer's protocol. Anti-Cas9 mouse monoclonal antibody (Cell Signaling Technology) was used to generate a standard curve, and the dilution gradient outlined in the manufacturer's instructions for the IgG mouse ELISA kit was used.

Western blotting. Human and mouse corneal tissues were ground using a TissueLyser with magnetic beads. Corneal suspensions and 293T cells were lysed in RIPA (Beyotime Biotechnology) supplemented with a protease inhibitor (Beyotime Biotechnology) for 30 min and incubated with SDS–PAGE sample loading buffer (Beyotime Biotechnology) for 15 min at 98 °C. Proteins were separated by SDS–PAGE and transferred to a PVDF membrane. The membrane was blocked with 5% nonfat milk dissolved in 0.05% Tween-20 in TBS for 1 h, cut according to the molecular weight marker and incubated with primary antibody overnight at 4 °C. Membranes were then incubated with anti-mouse secondary antibodies (1:3,000; Cell Signaling Technology, 4409) and visualized by hypersensitive ECL chemiluminescence (Beyotime Biotechnology) using a gel imaging system (Amersham ImageQuant 680, GE). β-actin was used for signal normalization across samples. The primary antibodies used in this experiment were anti-HSV VP5 monoclonal antibody (1:1,000; Santa Cruz Biotechnology, sc56989), anti-β-actin mouse monoclonal antibody (1:3,000; Cell Signaling Technology, 3700) and anti-Cas9 mouse monoclonal antibody (1:3,000; Cell Signaling Technology, 14697).

qPCR. Genomic DNA and total RNA from all samples were extracted using a viral DNA/RNA extraction kit (TaKaRa). cDNA was synthesized using the QuantScript RT kit (TIANGEN) according to the manufacturer's protocol. qPCR was performed using PowerUp SYBR Green Master Mix (Applied Biosystems) following the manufacturer's protocol. The qPCR experiments were performed using a real-time PCR system (LightCycler 96, Roche). To quantify HSV-1 genomes in mouse tissues or human corneas, genomic DNA and viral DNA were extracted from the corresponding parts of mice or human corneas and subjected to qPCR to detect HSV-1 (primers Y5/Y6), which was then normalized to mouse *Gapdh* (SK13/SK14) or human *GAPDH* (SK55/SK56). To detect mLP distribution in vivo, genomic DNA was extracted from the eye, TG, heart, liver, spleen, lung, kidney and testis. qPCR was performed to detect WPRE (primers SK9/SK10), which was then normalized to *Gapdh* (SK13/SK14). To detect the innate immune response induced by HELP and HSV-1 in mice, total RNA was extracted from eyes. RT–qPCR was performed to detect *Isg15* (SK51/SK52), *Ddx58* (encoding RIG-I; Y7/Y8) and *Ifnb1* (Y9/Y10), which were then normalized to *Gapdh* (Y23/Y24). To detect the innate immune response in human cells, RT–qPCR was performed to detect *ISG15* (Y11/Y12), *DDX58* (RIG-I; Y13/Y14) and *IFNB1* (Y15/Y16), which were then normalized to *GAPDH* (SK55/SK56). To measure the inflammatory molecules expressed in the cornea following HSV-1 infection, RT–qPCR was performed to detect *Il6* (Y17/Y18), *Ccl2* (Y19/Y20) and *Cxcl10* (Y21/Y22), which were then normalized to *Gapdh* (Y23/Y24). To detect the copy number of Cas9 mRNA in each HELP particle, the same amount of p24 for HELP and lenti-CRISPR was used to extract total RNA, which was then used to synthesize cDNA. RT–qPCR was performed using the SK11/SK12 primer pair. HELP data were normalized to lenti-CRISPR. The primer sequences used are listed in Supplementary Table 4.

Mice. Male 6- to 8-week-old specific-pathogen-free C57BL/6J mice were used in this study. Mice were housed in an environmentally controlled room maintained at 23 °C and 55% ± 5% humidity on a 12-h light/12-h dark cycle. HELP or PBS (mock) was injected into mice by intrastromal injection under a stereo light microscope (SMZ800N, Nikon). All mouse studies have complied with the guidelines of the Institutional Animal Care and Use Committee of the Shanghai Jiao Tong University with approval from the animal ethics committee.

Intrastromal injection. Mice were anesthetized, and a small intrastromal pocket was carefully created in the mid-peripheral cornea using a 29-gauge needle. A 33-gauge needle was then inserted toward the central cornea, and 2 μl of HELP or PBS was injected into the corneal stroma. Both eyes of each mouse were injected in this study. Mice were randomly allocated to experimental and control groups.

Acute HSV-1 infection mouse model. Mice were anesthetized by intraperitoneal injection of 1.25% Avertin, and corneas were scarified in a 3 × 3 cross-hatch pattern. Mice were then inoculated with 2×10^6 (or 5×10^4) p.f.u. of HSV-1 17syn+ on both eyes. Body weight and disease scores were measured at the indicated times after infection. Scoring was performed in a blinded manner using the following system: hair loss (0, none; 1, minimal periocular hair loss; 2, moderate periocular hair loss; 3, severe hair loss limited to the periocular region; 4, severe and extensive hair loss); hydrocephalus (0, none; 1, minor bump; 2, moderate bump; 3, large bump); symptoms related to neurological disease (0, normal; 1, jumpy; 2, uncoordinated; 3, hunched/lethargic; 4, unresponsive/no movement); eye swelling and lesions (0, none; 1, minor swelling; 2, moderate swelling; 3, severe swelling and skin lesions; 4, extensive lesions). Mice were killed at the specified time after infection. To collect eye swabs, mouse eyes were gently proptosed and then wiped with a sterile cotton swab (Miraclean Technology) three times around the eye in a circular motion and twice across the center of the cornea in a '+' pattern. The cotton swabs were placed in 1 ml of DMEM containing 2% (vol/vol) FBS and 1% P/S and stored at −80 °C until titered by plaque assay. Corneal graphs were collected using a color digital camera (DS-Ri2, Nikon) attached to a stereo light microscope (SMZ800N, Nikon) at the indicated time. Sera were collected at 14 d.p.i. to test for mouse humoral IgG specific to SpCas9 by ELISA.

Recurrent HSV-1 infection mouse model. Mice were inoculated with 2×10^5 p.f.u. of HSV-1 17syn+ in both eyes on scarified corneas. Mice that survived acute infection were maintained for 60 d, and disease was reactivated by UV-B irradiation of the eyes followed by HELP or PBS (mock) treatment. The TG and eyes were collected to quantify HSV-1 DNA by qPCR.

Human corneal HSV-1 infection. Human corneas were obtained from fresh cadavers and were supplied by the Eye Bank of the Eye, Ear, Nose and Throat Hospital, Fudan University, under the approval of the hospital ethics committee (EENTIRB-2017-06-07-01). Experiments were conducted according to the Declaration of Helsinki and in compliance with Chinese law. Corneas were evenly divided into two halves, and one half was dosed with 15 µl HELP by intrastromal injection (equal to 1.5 µg of p24) while the other (mock control) was dosed with PBS by intrastromal injection. Corneas were then infected with 2×10^6 p.f.u. of HSV-1 17syn+ in MEM containing 2% FBS. Medium was refreshed at 2 h.p.i. with MEM containing 10% FBS and 5% P/S. Two days after HSV-1 infection, corneas were processed for immunofluorescence imaging, immunoblotting or DNA isolation using the viral DNA extraction kit to quantify viral genomes by qPCR. The supernatants were collected for plaque assay.

Immunofluorescence imaging. For confocal imaging, 293T and mouse corneal stromal cells were imaged under a laser scanning confocal microscope (A1si, Nikon) at the indicated time. The eyes, TG and brain were fixed in 4% paraformaldehyde (PFA) overnight at 4 °C before transferring to 30% sucrose. The optimal cutting temperature (OCT) compound-embedded tissues were sectioned to 10-µm thickness using a freezing microtome (CM1950, Leica) and processed for immunofluorescence. Slides were dried at room temperature for 10 min and blocked in blocking buffer with 5% normal goat serum (Solarbio), 1% BSA and 0.3% Triton X-100 in PBS in a humidified box at room temperature for 30 min. Slides were incubated with primary antibody against HSV-1 VP5 (1:200; Santa Cruz Biotechnology, sc56989) or rabbit primary antibody against GFP (1:1,000; GeneTex, 113617) in 1% BSA overnight at 4 °C. After washing, the slides were incubated with anti-mouse secondary antibody (1:100; Santa Cruz Biotechnology, 516176) or anti-rabbit secondary antibody (1:500; Beyotime Biotechnology, a0468) in 1% BSA for 1 h. For whole-mount mouse corneal staining, freshly isolated mouse corneal buttons were cut from the eye globe on ice using a dissecting microscope. Corneal buttons were fixed in 4% PFA at 4 °C overnight and then washed in blocking buffer (1% BSA, 5% goat serum and 0.03% Triton X-100 in 1× PBS) for 1 h at room temperature. Corneas were incubated with primary anti-mouse β-III-tubulin antibody (1 µg ml^{-1}; Abcam, 238697) at 4 °C for 72 h and then washed thoroughly with washing buffer (0.05% Tween-20 in PBS). Corneas were incubated with corresponding secondary antibodies for 2 h at room temperature, washed and affixed to a coverslip. Fluorescent staining was imaged with a laser scanning confocal microscope (A1si, Nikon). The thickness of the *z* stacks generated for corneal whole mounts was 19 to 21 slices (4.2-mm step size).

Collagen-binding peptide staining. The 5-FAM-labeled N terminus of collagen-binding peptides (Cys-Gln-Asp-Ser-Glu-Thr-Arg-Thr-Phe-Tyr) was purchased from Sangon Biotech. Mouse eyes were frozen in OCT (Sakura Finetek) compound and cut into 15-µm-thick sections. The sections were blocked with PBS containing 5% donkey serum for 30 min at room temperature. Collagen-binding peptides were dissolved in PBS to obtain a final concentration of 50 ng µl^{-1}. Before staining, peptides were heated for 5 min at 80 °C in water and then immediately incubated on ice. Sections were then stained with peptide solution at 4 °C overnight. Following incubation, sections were rinsed three times with PBS. The samples were analyzed using a laser scanning confocal microscope (A1si, Nikon) at ×10 magnification.

Evaluation of corneal neovascularization. FITC–dextran with a molecular weight of 2×10^6 (Sigma-Aldrich) was diluted in saline to a concentration of 50 mg ml^{-1} before injection (0.15 ml) into the left ventricle of the mouse heart. Eyes were enucleated at 5 min after injection and fixed for 2 h with 4% PFA at 4 °C. Corneas were isolated under a stereo microscope with four radial incisions made to flatten each cornea on a slide. Slides were fixed for 10 min with 4% PFA and washed with PBS. The cornea was flattened on a glass slide and imaged using a laser scanning confocal microscope (A1si, Nikon).

Phenol red thread test. A 25-mm-long phenol red-impregnated thread with a 3-mm bent end was placed in the lower fornix of the mouse eye for 20 s. The phenol red thread changes color from yellow to red when it comes into contact with tears. The length of the red portion was measured with a ruler.

Cornea epithelial lesion test. Anesthetized mice were placed on a mouse holder, and the entire frame of the cornea was visible. A total volume of 4 µl of sodium fluorescein (0.5%) was added to the mouse eye. Images were captured in the cobalt blue channel with a surgical microscope (OPMI VISU S8, Carl Zeiss), and the stained area was quantified using ImageJ 1.52v software.

Electroretinography. Mice were adapted to the dark overnight and anesthetized by intraperitoneal injection of 1.25% Avertin. Corneal anesthesia and mydriasis were achieved with 0.5% proparacaine hydrochloride (Alcon-Couvreur) and 0.5% tropicamide (Alcon Laboratories). A thermal plate was used to maintain body temperature (37 °C). The full-field ERG was recorded from both eyes using an Espion Diagnosys system (Espion E2, Diagnosys). One subdermal needle was inserted into the tail acting as the ground electrode, while another subdermal needle placed over the nasal bone served as the reference electrode. Electrical signals were recorded with two 3-mm-diameter platinum wire loop electrodes placed on the corneal surface. Eyes were lubricated with 2.5% hydroxypropyl-methylcellulose solution (Gonak, Akorn). Light stimuli were delivered using a ColorDome unit. For dark-adapted responses, ERG was performed with a series of white flash stimuli ranging from 0.003 to 10 cd·s/m^2. A total of ten responses was averaged with interstimulus intervals (ISI) of 10 s. Mice subsequently underwent a 5-min period of light adaptation with a white background over which a series of flash stimuli (3, 10 and 30 cd·s/m^2) were superimposed (20 responses each, ISI = 2 s). The band-pass cutoff frequencies were 0.3 and 300 Hz. The data were analyzed using Espion software 6.0.54.

Deep sequencing. The top-ranked off-target sites in the mouse genome for *UL29*-targeting and *UL8*-targeting gRNAs were identified by the Cas-OFFinder online predictor. The on-target and predicted off-target sites were PCR amplified and pooled at an equal molar ratio for double-end sequencing using an Illumina MiSeq instrument at Novogene. Raw data for next-generation sequencing were analyzed by Cas-analyzer (version 2016.12.14). The primer sequences are listed in Supplementary Table 5.

Whole-genome sequencing. Genomic DNA from human corneas was isolated using a Magen HiPure Blood DNA Mini kit (AnGen Biotech). The purity, quantity and size of genomic DNA were assessed by NanoDrop and agarose gel electrophoresis. Genomic DNA was subjected to whole-genome DNA library preparation for high-throughput sequencing (Illumina platform) with a mean coverage of 51- and 45-fold for HELP- and mock-treated samples, respectively, in GENEWIZ. The Q30 was set above 85%, and the average error rate required was below 0.1%. Valid sequencing data were aligned to hg19 using Burrows–Wheeler Aligner 0.7.12. All polymorphic SNVs and indel sites in the genome were extracted, and high-confidence SNV and indel datasets were obtained and analyzed.

Prediction of potential off-target sites. The Cas-OFFinder tool was used to find all potential off-target sites based on sequence homology to either the *UL8* or *UL29* gRNA, allowing up to five mismatches. This resulted in 269 and 438 potential off-target sites being detected for *UL8* and *UL29*, respectively. These potential off-target sites were separated into coding, splicing, up- and downstream, noncoding RNA, 3′-UTR, 5′-UTR, intronic and intergenic regions. The 100 bp upstream and downstream of potential off-target sites were used to find SNVs and indels. The results were further filtered according to identity with the mock-treated samples, and repetitive sequences were excluded.

Histology. Mouse eyes were dissected and fixed in PFA before embedding in paraffin, sectioning at 10-µm thickness and staining with hematoxylin and eosin. For immunohistochemistry, the sections were deparaffinized and rehydrated, followed by incubation with citrate buffer for antigen retrieval. To block endogenous peroxidase activity, the sections were treated with 3% hydrogen peroxide for 25 min. The sections were then blocked with 3% BSA at room temperature for 30 min and incubated with anti-CD4 (1:100; Servicebio, gb13064), anti-CD8 (1:1,000; Servicebio, gb11068), anti-PD-L1 (1 µg ml^{-1}; Abcam, 238697), anti-CD11b (1:500; Servicebio, gb11058) and anti-F4/80 (1:500; Servicebio, gb11027) at 4 °C overnight. The slides were then incubated with an anti-rabbit secondary antibody (1:500; Servicebio, gb23303) or an anti-mouse secondary antibody (1:500; Servicebio, gb23301), followed by incubation with freshly prepared DAB substrate solution to detect antibody. The tissue was counterstained with hematoxylin, blued with ammonia water and then dehydrated and coverslipped. Images were collected using a fluorescence microscope (Eclipse Ni, Nikon).

Statistics. For in vitro studies, sample sizes were determined as triplicate samples or more for comparisons between one or multiple groups followed by the statistical test. Each experiment was repeated at least twice, and the experimental findings can be reliably reproduced. For in vivo studies, at least four mice were used for each group. Data are presented as mean ± s.e.m. in all experiments. Student's *t* tests, Mann–Whitney tests or one-way ANOVA was performed to determine the *P* values. The specific statistical method applied and a description of the replicates can be found in the figure legends. Asterisks and number signs indicate statistical significance ($^*P<0.05$, $^{**}P<0.01$, $^{***}P<0.001$; $^{\#}P<0.05$, $^{\#\#}P<0.01$, $^{\#\#\#}P<0.001$; NS, not significant). Statistics were analyzed with GraphPad Prism 8.

Reporting Summary. Further information on research design is available in the Nature Research Reporting Summary linked to this article.

Data availability

Data generated or analyzed during this study are available from the corresponding author on reasonable request. The deep-sequencing and whole-genome sequencing data are available at NCBI BioProject. The BioProject IDs are PRJNA668071 and PRJNA668060, respectively. Source data are provided with this paper.

Acknowledgements

We thank F. Zhang (MIT, USA) for reading and commenting on our manuscript. The work was supported by grants from the National Natural Science Foundation of China (31971364), the Pujiang Talent Project of Shanghai (18PJ1404500), the Natural Science Foundation of Shanghai (18ZR1419300) and startup funding from the Shanghai Center for Systems Biomedicine, Shanghai Jiao Tong University (WF220441504) to Y.C. and by the National Natural Science Foundation of China (81970766 and 81670818), the Shanghai Rising-Star Program (18QA1401100), the Shanghai Innovation Development Program (2020779) and the Shanghai Key Clinical Research Program (SHDC2020CR3052B) to J.H. S.R.P. is supported by the European Research Council (ERC-AdG ENVISION; 786602).

Author contributions

D.Y., S.L., J.H. and Y.C. conceptualized the study and designed the experiments; D.Y., S.L., D.W., Y.D., H.J. and X.Z. performed the experiments; S.R.P. provided the HSV-1 strains and facilitated building the mouse HSK model; all the authors analyzed the data; D.Y., S.L. and Y.C. wrote the manuscript with help from all the authors.

Competing interests

The authors declare no competing interests.

Additional information

Supplementary information is available for this paper at https://doi.org/10.1038/s41587-020-00781-8.

Correspondence and requests for materials should be addressed to J.H. or Y.C.

Peer review information *Nature Biotechnology* thanks Paul R. Kinchington and the other, anonymous, reviewer(s) for their contribution to the peer review of this work.

Reprints and permissions information is available at www.nature.com/reprints.

nature research

Corresponding author(s): Yujia Cai

Last updated by author(s): Nov 12, 2020

Reporting Summary

Nature Research wishes to improve the reproducibility of the work that we publish. This form provides structure for consistency and transparency in reporting. For further information on Nature Research policies, see our Editorial Policies and the Editorial Policy Checklist.

Statistics

For all statistical analyses, confirm that the following items are present in the figure legend, table legend, main text, or Methods section.

n/a	Confirmed	
☐	☒	The exact sample size (*n*) for each experimental group/condition, given as a discrete number and unit of measurement
☐	☒	A statement on whether measurements were taken from distinct samples or whether the same sample was measured repeatedly
☐	☒	The statistical test(s) used AND whether they are one- or two-sided *Only common tests should be described solely by name; describe more complex techniques in the Methods section.*
☒	☐	A description of all covariates tested
☐	☒	A description of any assumptions or corrections, such as tests of normality and adjustment for multiple comparisons
☐	☒	A full description of the statistical parameters including central tendency (e.g. means) or other basic estimates (e.g. regression coefficient) AND variation (e.g. standard deviation) or associated estimates of uncertainty (e.g. confidence intervals)
☐	☒	For null hypothesis testing, the test statistic (e.g. *F*, *t*, *r*) with confidence intervals, effect sizes, degrees of freedom and *P* value noted *Give P values as exact values whenever suitable.*
☒	☐	For Bayesian analysis, information on the choice of priors and Markov chain Monte Carlo settings
☒	☐	For hierarchical and complex designs, identification of the appropriate level for tests and full reporting of outcomes
☒	☐	Estimates of effect sizes (e.g. Cohen's *d*, Pearson's *r*), indicating how they were calculated

Our web collection on statistics for biologists contains articles on many of the points above.

Software and code

Policy information about availability of computer code

Data collection	No customized software was used; BD FACSDiva 7 was used to collect flow cytometry data; Roche LightCycler 96 Real-Time PCR system was used to collect real-time PCR data; Western blot data were collected by Amersham ImageQuant 680 system. Fluorescence images data were collected using Laser Scanning Confocal Microscope (A1si, Nikon). Hematoxylin-eosin staining and immunohistochemistry images data were collected using fluorescence microscope (Eclipse Ni, Nikon). Corneal graphs were collected using color digital camera (DS-Ri2, Nikon) attached to microscope (SMZ800N, Nikon). Cornea epithelial lesion images were captured with the surgical microscope (OPMI VISU S8, Carl Zeiss). The full-field electroretinography (ERG) was recorded using an Espion Diagnosys system (Espion E2, Diagnosys LLC).
Data analysis	GraphPad Prism 8, Cas-analyzer (version 2016.12.14), TIDE 2.0.1, ImageJ 1.52v, FlowJo 7.6, Espion software 6.0.54, Burrows-Wheeler Aligner 0.7.12.

For manuscripts utilizing custom algorithms or software that are central to the research but not yet described in published literature, software must be made available to editors and reviewers. We strongly encourage code deposition in a community repository (e.g. GitHub). See the Nature Research guidelines for submitting code & software for further information.

Data

Policy information about availability of data

All manuscripts must include a data availability statement. This statement should provide the following information, where applicable:

- Accession codes, unique identifiers, or web links for publicly available datasets
- A list of figures that have associated raw data
- A description of any restrictions on data availability

Data generated or analysed during this study are available from the corresponding author on reasonable request. The raw data of deep sequencing and whole genome sequencing are available at NCBI BioProject. The BioProject IDs are PRJNA668071 and PRJNA668060, respectively.

Field-specific reporting

Please select the one below that is the best fit for your research. If you are not sure, read the appropriate sections before making your selection.

☒ Life sciences ☐ Behavioural & social sciences ☐ Ecological, evolutionary & environmental sciences

For a reference copy of the document with all sections, see nature.com/documents/nr-reporting-summary-flat.pdf

Life sciences study design

All studies must disclose on these points even when the disclosure is negative.

Sample size	For in vitro experiments, sample sizes were determined by triplicate samples for comparisons between one or multiple groups, followed by the statistical test. For in vivo studies, at least four mice were used for each group. Sample sizes were chosen to meet or exceed the standards of reproducibility demonstrated in similar published studies.
Data exclusions	No data were excluded from analysis.
Replication	Reproducibility was verified. The replication details were noted in figure captions. Exact n number specified for each result.
Randomization	Samples were randomly allocated into experimental groups for in vitro experiments and animals were randomly grouped for in vivo experiments.
Blinding	For in vivo studies, the body weight and disease scores were measured as blinded study. Investigators were not blinded to the other studies.

Reporting for specific materials, systems and methods

We require information from authors about some types of materials, experimental systems and methods used in many studies. Here, indicate whether each material, system or method listed is relevant to your study. If you are not sure if a list item applies to your research, read the appropriate section before selecting a response.

Materials & experimental systems

n/a	Involved in the study
☐	☒ Antibodies
☐	☒ Eukaryotic cell lines
☒	☐ Palaeontology and archaeology
☐	☒ Animals and other organisms
☐	☒ Human research participants
☒	☐ Clinical data
☒	☐ Dual use research of concern

Methods

n/a	Involved in the study
☒	☐ ChIP-seq
☐	☒ Flow cytometry
☒	☐ MRI-based neuroimaging

Antibodies

Antibodies used

Antibodies used for ELISA:
Anti-Cas9 monoclonal antibody (Cell Signaling Technology, cat#14697) was diluted to make a standard curve, the diluted concentrations were 1000, 250, 62.5, 15.625, 3.906 and 0.976 ng/mL.

Antibodies used for western blotting:
Anti-HSV VP5 monoclonal antibody (Santa Cruz Biotechnology, cat: sc56989), 1:1000;
Anti-beta-actin mouse monoclonal antibody (Cell Signaling Technology, cat: 3700),1:3000;
Anti-Cas9 monoclonal antibody (Cell Signaling Technology, cat: 14697), 1:3000;
Anti-mouse secondary antibody (Cell Signaling Technology, cat: 4409), 1:3000.

Antibodies used for immunofluorescence:
Anti-HSV VP5 monoclonal antibody (Santa Cruz Biotechnology, cat: sc56989), 1:200;
Anti-GFP antibody (GeneTex, cat: 113617), 1:1000;
Anti-beta III-tubulin antibody (Abcam, cat: 238697), 1ug/mL;
Anti-mouse secondary antibody (Santa Cruz Biotechnology, cat: 516176), 1:100;
Anti-rabbit secondary antibody (Beyotime Biotechnology, cat: a0468), 1:500.

Antibodies used for immunohistochemistry:
Anti-CD4+ (Servicebio, cat: gb13064), 1:100;
Anti-CD8+ (Servicebio, cat: gb11068), 1:1000;
Anti-PD-L1 antibody (Abcam, cat: 238697), 1ug/mL;
Anti-CD11b antibody (Servicebio, cat: gb11058),1:500;

Anti-F4/80 antibody (Servicebio,cat: gb11027),1:500;
Anti-rabbit secondary antibody (Servicebio, cat: gb23303), 1:500;
Anti-mouse secondary antibody (Servicebio, cat: gb23301), 1:500.

Validation

Antibodies were from commercial sources and validated for each application by the manufacturers. Multiple dilutions were tested to determine the most appropriate dilution.
Anti-HSV VP5 monoclonal antibody (Santa Cruz Biotechnology, cat: sc56989): https://www.scbt.com/p/hsv-1-2-icp5-major-capsid-protein-antibody-3b6?requestFrom=search.
Anti-β-Actin mouse monoclonal antibody (Cell Signaling Technology, cat: 3700): https://www.cellsignal.com/products/primary-antibodies/b-actin-8h10d10-mouse-mab/3700.
Anti-GFP antibody (GeneTex, cat: 113617): https://www.genetex.cn/Product/Detail/GFP-antibody/GTX113617.
Anti-beta III-tubulin antibody (Abcam, cat: 238697): https://www.abcam.com/beta-iii-tubulin-antibody-tu-20-neuronal-marker-ab7751.html.
Anti-CD4+ (Servicebio, cat: gb13064): https://www.servicebio.com/html/Products/LabAntibodies/Monoclonals/640.html.
Anti-CD8+ (Servicebio, cat: gb11068): https://www.servicebio.com/html/Products/LabAntibodies/Polyclonals/1351.html.
Anti-PD-L1 antibody (Abcam, cat: 238697): https://doi.org/10.1186/s13027-020-00312-9.
Anti-CD11b antibody (Servicebio, cat: gb11058): https://www.servicebio.com/html/Products/LabAntibodies/Polyclonals/1339.html.
Anti-F4/80 antibody (Servicebio,cat: gb11027): https://www.service-bio.cn/goodsdetail?id=1330.
Anti-Cas9 monoclonal antibody (Cell Signaling Technology, cat: 14697) was against SpCas9 protein and applicable for all species as stated on the manufacturer's website: https://www.cellsignal.com/products/primary-antibodies/cas9-7a9-3a3-mouse-mab/14697?_=1605155532683&Ntt=14697&tahead=true. The validity of Anti-Cas9 monoclonal antibody was confirmed: https://doi.org/10.1016/j.ccell.2019.05.013.
Anti-Cas9 monoclonal antibody was validated by SpCas9 protein binding ELISA in our laboratory as the accurate standard curve, R^2=0.9614. The method was validated (https://doi.org/10.1089/hum.2015.087).

Eukaryotic cell lines

Policy information about cell lines

Cell line source(s)	293T, Vero, HaCaT, HaCaT IFNAR2-KO and THP-1 were obtained from the laboratory of Soren Riis Paludan. The commercial source of 293T, Vero, HaCaT and THP-1 was American Type Culture Collection (ATCC); Primary mouse corneal stromal cells were freshly isolated from C57BL/6J mice.
Authentication	None of the cell lines used were authenticated.
Mycoplasma contamination	All cell lines were tested negative for mycoplasma contamination.
Commonly misidentified lines (See ICLAC register)	No commonly misidentified cell lines were used in the study.

Animals and other organisms

Policy information about studies involving animals; ARRIVE guidelines recommended for reporting animal research

Laboratory animals	Six to eight weeks old, male, 20±1 gram, pathogen-free C57BL/6J mice were used in this study. Mice were housed in an environmentally controlled room (23 °C, with 55±5% humidity and 12 h/12 h light-dark cycle).
Wild animals	The study did not involve wild animals.
Field-collected samples	The study did not involve samples collected in the field.
Ethics oversight	All mice studies have complied with the guidelines of the Institutional Animal Care and Use Committee (IACUC) of the Shanghai Jiao Tong University with approval from the animal Ethics Committee.

Note that full information on the approval of the study protocol must also be provided in the manuscript.

Human research participants

Policy information about studies involving human research participants

Population characteristics	The corneas were obtained without knowing the human characteristics.
Recruitment	With the cadaver donors and their family's consent, donated corneas from the Eye Bank of Shanghai Eye, Ear, Nose and Throat Hospital, Fudan University, were obtained randomly.
Ethics oversight	Ethics committee of Shanghai Eye, Ear, Nose and Throat Hospital.

Note that full information on the approval of the study protocol must also be provided in the manuscript.

Flow Cytometry

Plots

Confirm that:

☒ The axis labels state the marker and fluorochrome used (e.g. CD4-FITC).

☒ The axis scales are clearly visible. Include numbers along axes only for bottom left plot of group (a 'group' is an analysis of identical markers).

☒ All plots are contour plots with outliers or pseudocolor plots.

☒ A numerical value for number of cells or percentage (with statistics) is provided.

Methodology

Sample preparation	Cells were fixed by 0.1 % paraformaldehyde in 4 °C overnight before analysis.
Instrument	LSR Fortessa flow cytometer (BD Biosciences).
Software	BD FACSDiva 7 was used to collect flow cytometry data; FlowJo 7.6 was used to analyze data.
Cell population abundance	10000 cells were aquired for analysis from each sample.
Gating strategy	Cells were identified by forward and side scatter, followed by doublet exclusion. Non-transduced cells were used as a negative control to draw boundaries between GFP positive and negative cells.

☒ Tick this box to confirm that a figure exemplifying the gating strategy is provided in the Supplementary Information.